Biogeosciences, 21, 3571–3592, 2024
https://doi.org/10.5194/bg-21-3571-2024

Biogeosciences Open Access EGU

Compound soil and atmospheric drought (CSAD) events and CO_2 fluxes of a mixed deciduous forest: the occurrence, impact, and temporal contribution of main drivers

Liliana Scapucci[1,★], Ankit Shekhar[1,★], Sergio Aranda-Barranco[2], Anastasiia Bolshakova[3], Lukas Hörtnagl[1], Mana Gharun[4], and Nina Buchmann[1]

[1]Department of Environmental Systems Science, ETH Zürich, Zurich, Switzerland
[2]Department of Ecology, University of Granada, Granada, Spain
[3]University of Natural Resources and Life Sciences Vienna (BOKU), Vienna, Austria
[4]Faculty of Geosciences, University of Münster, Münster, Germany
★These authors contributed equally to this work.

Correspondence: Liliana Scapucci (liliana.scapucci@usys.ethz.ch)

Received: 15 February 2024 – Discussion started: 26 February 2024
Revised: 30 May 2024 – Accepted: 7 June 2024 – Published: 13 August 2024

Abstract. With global warming, forests are increasingly exposed to "compound soil and atmospheric drought" (CSAD) events, characterized by low soil water content (SWC) and high vapour pressure deficit (VPD). Such CSAD events trigger responses in both ecosystem and forest-floor CO_2 fluxes, which we know little about. In this study, we used multi-year daily and daytime above-canopy (18 years; 2005–2022) and daily forest-floor (5 years; 2018–2022) eddy covariance CO_2 fluxes from a Swiss forest site by the name of CH-Lae (a mixed deciduous montane forest). The objectives were (1) to characterize CSAD events at CH-Lae, (2) to quantify the impact of CSAD events on ecosystem and forest-floor CO_2 fluxes, and (3) to identify the major drivers and their temporal contributions to changing ecosystem and forest-floor CO_2 fluxes during CSAD events and CSAD growing seasons. Our results showed that the growing seasons of 2015, 2018, and 2022 were the three driest at CH-Lae since 2005 (referred to as the CSAD years), exhibiting similar intensity and duration of the CSAD events but considerably different pre-drought conditions. The CSAD events reduced daily mean net ecosystem productivity (NEP) in all 3 CSAD years by about 38 % compared to the long-term mean, with the highest reduction observed during 2022 (41 %). This reduction in daily mean NEP was largely due to decreased gross primary productivity (GPP; > 16 % below the long-term mean) rather than increased ecosystem respiration (Reco) during CSAD events. Furthermore, forest-floor respiration (Rff) decreased during the CSAD events in 2018 and 2022 (with no measurements in 2015), with a larger reduction in 2022 (41 %) than in 2018 (16 %), relative to the long-term mean (2019–2021). Using data-driven machine learning methods, we identified the major drivers of NEP and Rff during CSAD events. While daytime mean NEP (NEP_{DT}) during the 2015 and 2018 CSAD events was limited by VPD and SWC, respectively, NEP_{DT} during the 2022 CSAD event was strongly limited by both SWC and VPD. Air temperature had negative effects, while net radiation showed positive effects on NEP_{DT} during all CSAD events. Daily mean Rff during the 2018 CSAD event was driven by soil temperature and SWC but was severely limited by SWC during the 2022 CSAD event. We found that a multi-layer analysis of CO_2 fluxes in forests is necessary to better understand forest responses to CSAD events, particularly if the first signs of NEP acclimation to CSAD events – evident in our forest – are also found elsewhere. We conclude that CSAD events have multiple drivers with different temporal contributions, making predictions about site-specific CSAD events and long-term forest responses to such conditions more challenging.

Published by Copernicus Publications on behalf of the European Geosciences Union.

1 Introduction

Forests play an essential role in mitigating climate change thanks to their ability to partially offset anthropogenic CO_2 emissions (Harris et al., 2021). However, the increasing frequency of droughts and heatwaves is compromising the carbon uptake capacity of forests worldwide (Anderegg et al., 2022). According to the Intergovernmental Panel on Climate Change (IPCC, 2023), the temperature increase over Europe (1850–1990) has been about twice the global mean since the pre-industrial period, accompanied by an increase in frequency of drought events (Spinoni et al., 2018). Recent studies have revealed that European forests are experiencing increasing rates of tree mortality induced by low soil water content (SWC) (George et al., 2022). In addition, recent studies have highlighted the role of high vapour pressure deficit (VPD), an indicator of atmospheric drought and a distinct characteristic of heatwaves, in further exacerbating tree mortality (Birami et al., 2018; Gazol and Camarero, 2022; Grossiord et al., 2017, 2020). Due to enhanced land–atmosphere feedback in response to climate change, the frequency of co-occurring low-soil-moisture and high-VPD conditions has also increased (Dirmeyer et al., 2021; Miralles et al., 2019; Orth 2021; Zhou et al., 2019), resulting in so-called "compound soil and atmospheric drought" (CSAD) conditions. The European droughts of 2003, 2015, and 2018, as well as the most recent one in 2022, were indeed characterized by CSAD conditions (Dirmeyer et al., 2021; Ionita et al., 2021, 2017; Lu et al., 2023; Tripathy and Mishra, 2023). In 2022, Europe experienced its hottest and driest year on record, with the summer being the warmest ever recorded, which ultimately led to numerous CSAD events across the continent (Copernicus Climate Change Service, 2023).

Such CSAD events have multiple impacts on forest ecosystems. They can reduce net ecosystem productivity (NEP) by decreasing gross primary productivity (GPP) and/or increasing ecosystem respiration (Reco) (Xu et al., 2020). Additionally, soil respiration (SR) can be reduced due to water scarcity in the soil, which limits both heterotrophic and autotrophic respiration (Ruehr and Buchmann, 2010; Ruehr et al., 2010; van Straaten et al., 2011; Sun et al., 2019; Schindlbacher et al., 2012). However, high soil temperature (TS) can increase SR rates when soil moisture is not limiting metabolic reactions in the soil (Schindlbacher et al., 2012), thereby affecting the sensitivity of respiration to soil temperature (Sun et al., 2019). Thus, to better understand the ecological consequences of climate change on forest ecosystems, it is crucial to assess how forests acclimate to stress conditions, such as CSAD events – for example, through changes in NEP sensitivity to abiotic drivers (e.g. air temperature (Tair), VPD, and SWC) during a growing season or across growing seasons (Grossman, 2023).

The summer of 2022 in Europe, characterized by strong CSAD conditions (Tripathy and Mishra, 2023; van der Woude et al., 2023), saw an extensive reduction in forest greenness (about 30 % of temperate and Mediterranean European forest area; Hermann et al., 2023) and a reduction in GPP (van der Woude et al., 2023), comparable to CSAD events during the summer of 2018. In 2018, this resulted in drought-induced tree mortality in Scots pine (*Pinus sylvestris* L.) and European beech (*Fagus sylvatica* L.) forests (Haberstroh et al., 2022; Obladen et al., 2021; Rukh et al., 2023; Schuldt et al., 2020). Clearly, most drought impact studies use data measured above the canopy, e.g. net carbon dioxide (CO_2) exchange or remote sensing of vegetation. Notably, the latter largely neglects the below-canopy component of the forest (also known as the forest floor), although it might show contrasting responses to drought conditions compared to the top canopy, which is sensed from above (Chi et al., 2021). The forest floor, composed of soil, tree roots, woody debris, and understory vegetation, provides an essential interface for soil–atmosphere CO_2 exchange, with photosynthesis of understory vegetation and forest-floor respiration (Rff) both representing major CO_2 exchange processes (Chi et al., 2021; Paul-Limoges et al., 2017). Therefore, separating the ecosystem-level drought response from the forest-floor drought response provides a more comprehensive insight into drought impacts than examining just one level alone (Chi et al., 2017; Martinez-Garcia et al., 2022). Furthermore, the intensity and duration of CSAD events, as well as their impacts on forests, can largely vary at a regional scale (Pei et al., 2013; Kim et al., 2020). Thus, more attention is needed on temperate-forest ecosystems in countries across Central Europe, such as in Switzerland, where forests are accustomed to cool, humid climates with an ample amount of summer rainfall (Schuldt and Ruehr, 2022).

In Switzerland, 2022 was the warmest year on record since instrumental measurements began in 1864, with average air temperatures reaching 1.6 °C above the long-term mean (1991–2020) and annual precipitation amounting to only 60 % of the long-term average (MeteoSvizzera, 2023). Such hot and dry conditions, as observed in 2022, were likely to result in CSAD events, potentially compromising the CO_2 uptake capacity of forests. Thus, the objectives of this study were (1) to characterize CSAD events at a Swiss mixed deciduous montane forest site, (2) to quantify the impact of CSAD events on ecosystem and forest-floor CO_2 fluxes, and (3) to identify the major drivers of ecosystem and forest-floor CO_2 fluxes and their temporal contributions during CSAD events and CSAD growing seasons.

2 Material and methods

2.1 Forest site

The study was conducted in a managed mixed deciduous montane forest located at a site in Lägeren (CH-Lae; 682 m a.s.l.). This site is situated in the far east of the Jura Mountains in Switzerland. The CH-Lae forest has a com-

plex canopy structure with a rather high species diversity. The dominant species are European beech (*Fagus sylvatica* L.; 40 % cover), ash (*Fraxinus excelsior* L.; 19 % cover), sycamore maple (*Acer pseudoplatanus* L.; 13 % cover), European silver fir (*Abies alba* Mill.; 8 % cover), large-leaved linden (*Tilia platyphyllos* Scop.; 8 %), and Norway spruce (*Picea abies* (L.) H. Karst.; 4 % cover) (Paul-Limoges et al., 2020). The forest shows no significant trend in leaf area index (LAI) over the years. The soils at CH-Lae are characterized by two main types, Rendzic Leptosols and Haplic Cambisols, with bedrock consisting of limestone marl, sandstone, and transition zones between the two (Ruehr et al., 2010). The mean annual air temperature at CH-Lae was 8.8 ± 1.3 °C (mean $\pm$ SD), and the mean annual precipitation was 831 ± 121 mm from 2005–2022. The understory vegetation at CH-Lae is dominated by wild garlic (*Allium ursinum* L.; height: ~ 30 cm), which grows for a short period in spring and early summer (March–June; Ruehr and Buchmann, 2009). The net carbon uptake period at CH-Lae is from May to September (Fig. A1).

2.2 Ecosystem-level measurements

In this study, we used measurements of ecosystem CO_2 fluxes from above the forest canopy, employing the eddy covariance (EC) technique (Aubinet et al., 2012), for the years from 2005–2022. The EC system (eddy tower coordinates: 47°28′42.0″ N, 8°21′51.8″ E) was mounted at a height of 47 m (mean canopy height: 30 m) above the ground. The EC technique utilizes high-frequency (20 Hz) measurements of wind speed and wind direction, measured with a three-dimensional sonic anemometer, and gas concentration (here CO_2 concentration), measured with an infrared gas analyser (IRGA) as CO_2 molar density (using an open-path IRGA from 2004–2015) or as a dry mole fraction (using a closed-path IRGA from 2016–2022; for details of the instrumentation used in the EC system, see Table A1). The time lag between turbulent fluctuations in vertical wind speed and CO_2 molar density (or the dry mole fraction) was calculated using covariance maximization (Fan et al., 1990). Half-hourly fluxes of CO_2 (FCs; $\mu mol\, CO_2\, m^{-2}\, s^{-1}$) were then calculated from the 20 Hz measurements using v7.0.9 of the EddyPro software (LI-COR, Inc., Lincoln, NE, USA), following established community guidelines (Aubinet et al., 2012; Sabbatini et al., 2018). The FCs from the open-path IRGA, LI-7500, were corrected for air density fluctuations (Webb et al., 1980). All FCs underwent spectral corrections for high-pass-filtering (Moncrieff et al., 2004) and low-pass-filtering (Fratini et al., 2012; Horst, 1997) losses. The impact of self-heating of the open-path IRGA on FCs was corrected based on a method described by Kittler et al. (2017). The net ecosystem exchange (NEE) of CO_2 was calculated as the sum of the FCs and the CO_2 storage term estimated from concentrations based on one-point measurements (Greco and Baldocchi, 1996). The quality of half-hourly NEE flux values was ensured by applying a comprehensive quality-screening process that combined several well-tested methods into a single quality flag (0–1–2 system; Mauder and Foken, 2006; Sabbatini et al., 2018). Fluxes with a low quality (i.e. a flag value of 2) were removed from further analyses. Fluxes that passed the quality-screening process were then gap-filled (Reichstein et al., 2005) and partitioned into gross primary productivity (GPP) and ecosystem respiration (Reco) using the daytime-partitioning method (Lasslop et al., 2010). More details about quality screening, filling gaps, and partitioning can be found in Shekhar et al. (2024). In this study, we used net ecosystem productivity (NEP $= -$NEE) for further data analyses. Positive NEP fluxes represent CO_2 uptake by the forest, whereas negative NEP represents CO_2 release. Along with fluxes, we also measured half-hourly Tair, relative humidity (RH), incoming shortwave radiation (Rg), and precipitation (Precip) at the top of the EC tower from 2005–2022 (see Table A1 for instrumentation details). We estimated half-hourly VPD from half-hourly measurements of air temperature and relative humidity.

2.3 Forest-floor measurements

We measured forest-floor CO_2fluxes using the EC technique (Aubinet et al., 2012) below the canopy from 2018 to 2022 to estimate the net ecosystem exchange of forest-floor (NEE_{ff}), which includes CO_2 fluxes from the soil and understory vegetation. We partitioned NEE_{ff} into the gross primary productivity of the forest floor (GPP_{ff}) and the respiration of the forest floor (Rff; Lasslop et al., 2010). The below-canopy station at CH-Lae was located ca. 100 m from the main tower (47°28′42.9″ N, 8°21′27.6″ E) and had a height of 1.5 m. Wind speed and direction were measured with a sonic anemometer, and CO_2 concentrations were measured with an open-path IRGA (LI-7500; Table A1) at a frequency of 20 Hz. We calculated NEE_{ff} and the partitioned fluxes using the same process and corrections as for above-canopy measurements (with the exception of the self-heating correction). We used seasonal u* filtering to account for changes in the understory canopy, with values of $0.024\, m\, s^{-1}$ for spring (days 60–151), $0.027\, m\, s^{-1}$ for summer (days 152–243), $0.039\, m\, s^{-1}$ for autumn (days 244–334), and $0.025\, m\, s^{-1}$ for winter (days 335–60). Additionally, we continuously measured the air temperature ($Tair_{ff}$), relative humidity (RH_{ff}), incoming shortwave radiation (Rg_{ff}), soil temperature (TS) and soil water content (SWC) at depths of 5, 10, 20, 30, and 50 cm at the forest-floor meteorological station next to the below-canopy EC system (Table A1). In 2020, we installed an additional soil moisture profile. To account for spatial heterogeneity, we normalized the SWC data using a z-score transformation and then used the z scores of SWC for further analyses.

2.4 Soil respiration measurements

Moreover, 10 PVC collars (diameter: 20 cm; height: 13 cm; depth: 2 cm) were installed at CH-Lae in spring 2022. They were installed at the same locations within the footprint of the tower as described in Ruehr et al. (2010). Soil respiration (SR) measurement campaigns were performed at least once a month from March to November 2022 using an LI-8100-103 analyser and a closed chamber (Table A1). Collars were measured once a day in a random order during each campaign. Each measurement lasted 90 s from the moment the chamber of the instrument was closed on top of the collar. Next to each collar, we measured SWC_S (SWC from survey measurements) at 5 cm with a soil moisture sensor and TS_S (TS from survey measurements) at 5 cm with a temperature sensor (Table A1). When the Swiss meteorological service (MeteoSwiss) forecasted a 2-week heatwave starting on 14 July 2022, we intensified the SR measurements to one campaign every second day, with two rounds of measurements per day (at 09:00 and at 16:00 LT) for 2 weeks. The order of measurements was inverted each fieldwork day. Since the portable soil moisture sensor broke on 22 July 2022 and was unavailable until 11 August 2022, we calculated the SWC for these days based on continuous measurements from the forest-floor meteorological station ($SWCs = 1.34 \cdot SWC - 10.7$; $R^2 = 0.82$).

2.5 Data analyses

In this study, we focused our analyses on the growing season, between May and September, when the long-term mean of ecosystem NEP (2005–2022) was positive, indicating that the GPP of the vegetation overcompensated for all respiratory losses (Fig. A1; Körner et al., 2023). We conducted all data analyses using the R programming language (version 4.3.3; R Core Team, 2021). We compared cumulative precipitation (indicating the total water supply to the forest) and cumulative VPD (indicating the total atmospheric water demand) during the growing seasons of 18 years at our forest site and chose the 3 years with the driest growing seasons, i.e. those with low cumulative precipitation and high VPD (referred to hereafter as CSAD years). Then, we identified CSAD events during these CSAD years as periods when both the soil and atmosphere were significantly drier than usual for more than 10 consecutive days, indicating compound drought conditions. To identify drier-than-usual periods, we compared 5 d daily moving means (assigned to the centre of the 5 d period) of SWC and VPD with their long-term (2005–2022) means. Therefore, a CSAD event was identified as a period of 10 consecutive days or more where the SWC was significantly lower ($p < 0.05$) and the VPD was significantly higher ($p < 0.05$) than the long-term mean.

We quantified the impact of CSAD events based on anomalies in NEP, GPP, Reco, and Rff by comparing them with their respective long-term means – for NEP, GPP, and Reco, the mean was calculated for 2005–2022, while for Rff, the mean was calculated for 2019–2021. Since CSAD events occurred in 2 of the 5 years of flux data available at the forest-floor station (Rff), we excluded 2018 and 2022 from the calculation of the Rff long-term mean. To understand the major drivers of NEP and Rff, we performed two different driver analyses in this study, with the first focusing on the CSAD years and the second focusing on the CSAD events in the CSAD years.

1. For the first driver analysis, we used a conditional-variable-importance (CVI) feature based on a random forest regression model (Breiman, 2001). For modelling daily mean NEP, the predictors were Rg, VPD, and Tair measured above the canopy, as well as SWC measured at the forest-floor station, whereas for modelling daily mean Rff, the predictors were Rg (Rg_{ff}), Tair ($Tair_{ff}$), soil temperature (TS), SWC, measured at the forest-floor station. The model was run separately for each year. CVI is specifically designed to consider multi-collinearity among predictors (i.e. Tair, VPD, and Rg) while estimating the importance of each predictor variable (Strobl et al., 2008), and it is thus considered a very reliable method for estimating overall feature importance. To estimate CVI, we used the "cforest" and "varimp" functions from the R package "party" (Hothorn et al., 2006).

2. For the second driver analysis, we used daytime mean NEP (NEP_{DT}), excluding nighttime data to highlight the effects of environmental drivers when photosynthesis dominates, to avoid potential biases that could arise if GPP were used since some predictors (i.e. Tair and Rg) were used to partition NEE into GPP and Reco. We used a TreeExplainer-based SHapley Additive exPlanations (SHAP) framework (Lundberg and Lee, 2017; Lundberg et al., 2020) with a tree-based ensemble-learning eXtreme Gradient Boosting (XGB) model (Chen and Guestrin, 2016). The XGB model was used to model NEP_{DT} and Rff, applying GridSearchCV methodology to optimize the parameters of the XGB model for NEP and Rff (for more details, see Wang et al., 2022). The TreeExplainer-based SHAP framework integrates explanatory models (here, the XGB model) with game theory (Shapley, 1953), which allowed us to estimate the marginal contribution (known as the SHAP value) of each predictor variable (i.e. Tair, VPD, SWC, and TS) to the response variables (NEP_{DT} and Rff). We used the "xgboost" (eXtreme Gradient Boosting) function from the R package "xgboost" to train the model, and we used the functions "shap.values" and "shap.prep" from the R package "SHAPforxgboost" (Chen and Guestrin, 2016) to obtain the SHAP values of each predictor variable for NEP_{DT} (2005–2022) and Rff (2018–2022). The models were run separately for each year, and we obtained the marginal contributions of each feature for each day

of each growing season, which allowed us to observe their temporal course. Then, we calculated the mean SHAP value during the CSAD events for each predictor of NEP_{DT} and Rff across the CSAD years to determine the dominant direction of the effect of each feature. To determine the differences from the long-term means, we also calculated the mean SHAP values of the predictors during the respective reference periods – for NEP_{DT}, the long-term mean was calculated for 2005–2022, while for daily Rff, it was calculated for 2019–2021. The reference periods included all days on which a CSAD event occurred, independent of the year, i.e. from 7 July to 23 August for NEP_{DT} during 2005–2022 (including CSAD years due to the large number of years with measurements available) and from 14 July to 23 August for Rff during 2019–2021 (excluding CSAD years due to the small number of years with measurements available; Fig. A2). For comparison with the first model (based on CVI), we also calculated the mean and standard error of the absolute SHAP values for NEP in 2015, 2018, and 2022, as well as the long-term mean for 2005–2022 (Fig. A3). However, since we were interested in short-term changes in driver importance, including changes in the direction of their effect, we did not follow up with absolute SHAP values in this study.

We then used the SHAP values of the drivers (VPD, Tair, and SWC for NEP_{DT}; TS and SWC for Rff) to estimate the acclimation of NEP_{DT} and Rff to abiotic drivers. This was done by estimating the absolute driver values (thresholds) related to the largest effects, as indicated by the maximum marginal contributions to the response variables NEP_{DT} and Rff in each CSAD year (Gou et al., 2023; Wang et al., 2022). For this, we fitted a local polynomial regression between the SHAP values of the driver variable and the driver variable itself, i.e. a loess curve, and calculated the residual standard error from the loess function of the "stats" R package. We then identified the absolute driver value corresponding to the highest SHAP values (feature_NEP_{max} and feature_Rff_{max}) for each CSAD year (i.e. VPD_NEP_{max}, Tair_NEP_{max}, and SWC_NEP_{max}); the VPD, Tair, and SWC values associated with the highest marginal contributions to NEP_{DT}; and TS_Rff_{max} and SWC_Rff_{max}, which are the TS and SWC values associated with the highest marginal contributions to Rff. These absolute driver values provided information about NEP_{DT} and Rff sensitivities to abiotic drivers during the growing season of each CSAD year. For example, a shift in SWC_NEP_{max} towards drier conditions in one growing season compared to that in other growing seasons translated into an acclimation of NEP_{DT} to drier conditions in that growing season. To test if the feature_NEP_{max} values varied with the corresponding mean feature values during the respective growing seasons, we fitted a linear regression between the mean VPD, SWC, and Tair and their corresponding values of NEP_{max} for each year from 2005 to 2022.

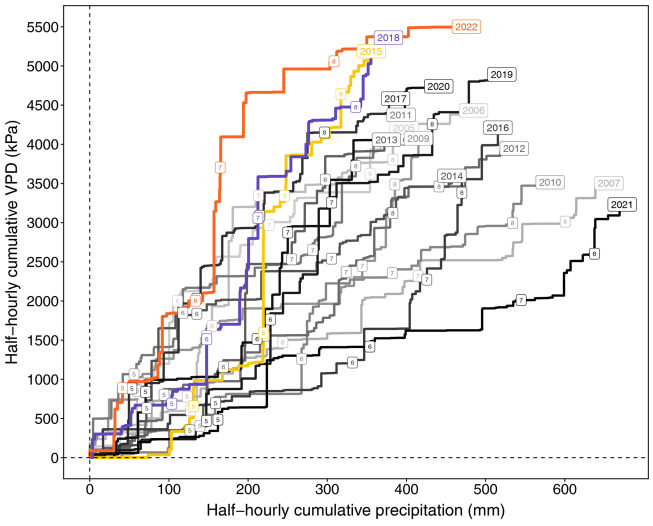

Figure 1. Cumulative VPD and cumulative precipitation from May to September (the growing season of the Lägeren forest) of each year (2005–2022). The numbers (5–9) on the cumulative lines each indicate the end of each month.

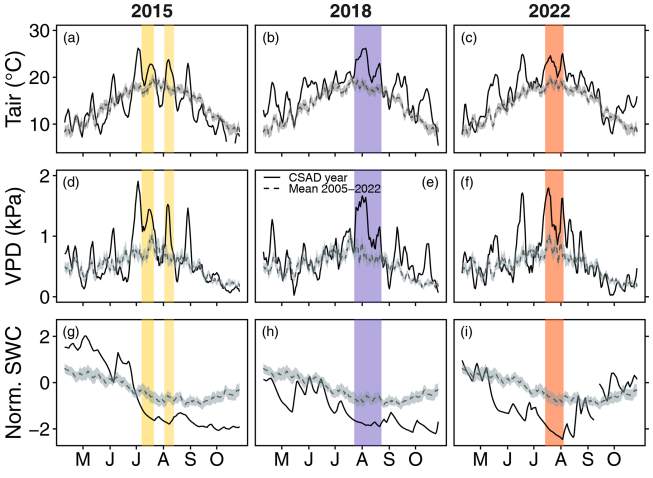

Figure 2. Comparison of 5 d moving averages of daily mean **(a–c)** Tair, **(d–f)** VPD, and **(g–i)** SWC for the years with a CSAD event against the long-term means (2005–2022). The band around the dashed line indicates the standard error of the long-term mean (2005–2022). The coloured areas highlight the CSAD events, i.e. periods with the lowest SWC and highest VPD occurring simultaneously. "Norm. SWC": normalized SWC. The *x* axes show the months of the year from May to October.

Finally, we used linear models to explain daily mean SR responses to TS and SWC during the CSAD events and the rest of the years, based on measurements from the survey campaigns in 2022. The amount of SR data was not sufficient to apply machine learning approaches.

3 Results

3.1 Detected CSAD events

The growing seasons (May to September) of 2015, 2018, and 2022 were the three driest in the last 18 years (2005–2022) at the mountain forest site (Fig. 1). The growing seasons in these 3 years were characterized by very high atmospheric drought (indicated by cumulative VPD) and low water supply (indicated by cumulative precipitation, a proxy for soil drought) In particular, the summer months (June–August) of these 3 years were significantly warmer and drier (Fig. 1 and 2). Mean summer temperatures for 2018 (19.8 °C) and 2022 (20.3 °C) were more than 2.5 °C higher than the long-term mean summer temperature at the forest site (17.2 °C). Summer precipitation in 2018 and 2022 was more than 20 % and 10 % lower, respectively, than the long-term mean cumulative summer precipitation (300 mm). Furthermore, in July of 2015 and 2022, less than one-third of the long-term mean cumulative summer precipitation was recorded. Coupled with an increase in average VPD greater than 50 % , this resulted in intense soil-drought and atmospheric-drought conditions.

Moreover, in 2015, we detected two distinct CSAD events, i.e. periods of 10 or more consecutive days with significantly lower SWC and significantly higher VPD than the long-term mean – one event from 7 to 21 July 2015 and a second event from 2 to 13 August 2015 (Fig. 2a, d, and g). These events lasted a total of 27 d, with a mean maximum temperature of 26.9 °C, a mean maximum VPD of 2.24 kPa, and a mean minimum normalized SWC of −1.83 (Table 1). For comparison, in 2018, the CSAD event lasted 32 d, from 23 July 2018 to 23 August 2018 (Fig. 2b, e, and h), with a mean maximum temperature of 27.7 °C, a mean maximum VPD of 2.19 kPa, and a mean minimum normalized SWC of −1.94 (Table 1). In 2022, the CSAD event lasted 22 d, from 14 July 2022 to 4 August 2022. Thus, although it was shorter than the 2015 and 2018 CSAD events (Fig. 2c, f, and i), it was more intense, with a mean maximum temperature of 28.3 °C, a mean minimum VPD of 2.43 kPa, and a mean minimum normalized SWC of −2.51 (Table 1). We measured the highest air temperature (33.56 °C) and the third-highest VPD (3.83 kPa) ever recorded at the forest site over the past 18 years (2005–2022) on the last day of the 2022 CSAD event, i.e. on 4 August 2022 between 16:30 and 17:00 LT (Fig. A4). Furthermore, the 2022 CSAD event was characterized by multiple tropical nights (where nighttime temperatures exceeded 20 °C; Fig. A4) and progressive soil drying (Fig. 2).

Thus, the CSAD events slightly differed not only in terms of intensity but also in terms of the timing of the events (Table 1) and initial drought development. In 2015 and 2018, wetter soil conditions (compared to the long-term mean; 2015) or normal soil conditions (2018) continued from late spring (mid-May) until the end of June, followed by a quick soil-drought intensification in July due to high air temperatures (> 30 °C), high VPD (> 3.8 kPa) (Fig. 2), and low precipitation (more than 40 % below the long-term July average). However, 2022 was characterized by exceptionally low soil water content and high VPD (> 2.5 kPa) as early as May (Fig. 2i). This condition intensified with low precipitation and high temperatures into early summer. Nighttime VPD exceeded 2 kPa on a few days in June, preceding the CSAD event that occurred from mid-July to the beginning of August (see Fig. A4). Even the heavy rainfall on 5 August 2022 (28 mm) only resulted in a minor increase in SWC. Nevertheless, after 4 August 2022, air temperature and VPD had returned to near-normal conditions, marking the end of the 2022 CSAD event (Fig. 2).

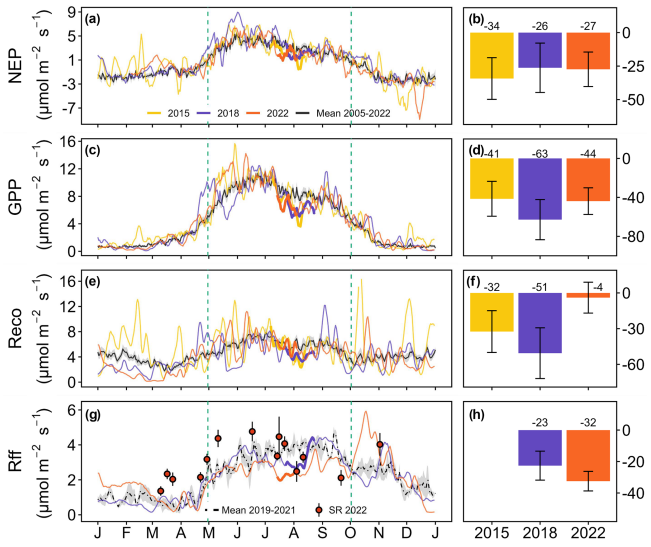

Figure 3. Comparison of daily mean **(a)** net ecosystem productivity (NEP), **(c)** gross primary productivity (GPP), **(e)** ecosystem respiration (Reco), and **(g)** forest-floor respiration (Rff) for the years when a CSAD event occurred (2015, 2018, and 2022) against their respective long-term means (**a**, **c**, **e**, **g**). The grey bands around the long-term means each represent the standard error of the respective long-term mean CO_2 fluxes. Soil respiration (SR) measurements, given as daily means (± SD), were measured manually in 2022 only. The thicker lines represent CSAD events. The right-hand panels (**b**, **d**, **f**, and **h**) show the cumulative difference between the actual fluxes recorded during a CSAD event and the respective long-term mean fluxes (2005–2022 for NEP, GPP, and Reco; 2019–2021 for Rff). The associated error bars show the cumulative standard errors of the long-term mean CO_2 fluxes for the respective CSAD events.

3.2 Impacts of CSAD events on CO_2 fluxes

All CSAD events had immediate negative impacts on ecosystem CO_2 fluxes, showing a decrease in CO_2 fluxes compared to the long-term means (Table 2; Fig. 3a, c, e, and g). The daily mean NEP, GPP, Reco, and Rff tended to be lower during CSAD events compared to their respective long-term means for the reference periods of 2005–2022 (for NEP, GPP,

Table 1. Characterization of CSAD events in 2015, 2018, and 2022. The table provides the duration in days; the maximum (max) and standard deviation (± SD) of daily mean Tair; the maximum (max) and standard deviation (± SD) of daily mean VPD; and the minimum (min) and standard deviation (± SD) of daily mean normalized SWC. All data were recorded during the CSAD events of 2015, 2018, and 2022.

Year	Duration (d)	Max ± SD Tair (°C)	Max ± SD VPD (kPa)	Min ± SD SWC (normalized)
2015	15 + 12 = 27	26.9 ± 3.03	2.24 ± 0.4	−1.83 ± 0.20
2018	32	27.7 ± 2.88	2.19 ± 0.5	−1.93 ± 0.10
2022	22	28.3 ± 2.64	2.43 ± 0.5	−2.51 ± 0.20

Table 2. Daily mean CO_2 fluxes during CSAD events in 2015, 2018, and 2022, as well as the long-term means for the respective reference periods. The table provides the means and standard deviations of net ecosystem productivity (NEP), partitioned gross primary productivity (GPP), ecosystem respiration (Reco), and forest-floor respiration (Rff). The reference periods for NEP, GPP, and Reco each includes all days from 7 July to 23 August from 2005 to 2022. The reference period for Rff includes all days from 14 July to 23 August from 2019 to 2021. All fluxes are given in $\mu mol\,CO_2\,m^{-2}\,s^{-1}$.

	NEP	GPP	Reco	Rff
CSAD 2015	2.09 ± 2.14	7.33 ± 2.54	5.05 ± 2.11	NA
CSAD 2018	1.99 ± 1.36	6.31 ± 1.44	4.23 ± 0.89	3.19 ± 0.68
CSAD 2022	1.89 ± 1.77	6.69 ± 1.33	5.73 ± 1.55	2.24 ± 0.20
Reference period	3.2 ± 0.82	8.77 ± 0.85	6.14 ± 0.65	3.81 ± 0.26

NA: not available.

and Reco) and 2019–2021 (for Rff; Table 2). The lowest average NEP was recorded during the CSAD event of 2022 (a decrease of 41 %), followed by decreases in NEP of 38 % and 35 % during the 2018 and 2015 CSAD events, respectively. Moreover, the lowest average GPP and Reco were found during the 2018 CSAD event (decreases of 28 % and 31 %, respectively; Table 2).

All cumulative CO_2 fluxes decreased during CSAD events in 2015, 2018, and 2022 compared to the long-term means (Fig. 3b, d, f, and h), with the exception of Reco in 2022. Cumulative NEP during the CSAD events in 2015 and 2018 decreased by 34 and 26 $\mu mol\,CO_2\,m^{-2}\,s^{-1}$, respectively, compared to the long-term mean of the reference period (2005–2022; Fig. 3b). During the CSAD years of 2015 and 2018, cumulative GPP and Reco decreased considerably, although cumulative GPP tended to decrease more ($> 40\,\mu mol\,CO_2\,m^{-2}\,s^{-1}$) than Reco ($> 30\,\mu mol\,CO_2\,m^{-2}\,s^{-1}$; Fig. 3d and f). In contrast, during the 2022 CSAD event, cumulative NEP decreased by 27 $\mu mol\,CO_2\,m^{-2}\,s^{-1}$ compared to the long-term mean (Fig. 3b); this was due to a decrease in cumulative GPP (by 44 $\mu mol\,CO_2\,m^{-2}\,s^{-1}$) and negligible changes in Reco (Fig. 3d and f). Furthermore, Rff fluxes during the 2018 and 2022 CSAD events were lower compared to the long-term mean of the reference period (2019–2021), with decreases of 23 and 32 $\mu mol\,CO_2\,m^{-2}\,s^{-1}$, respectively (Fig. 3h). These decreases in Rff were supported by decreasing daily mean SR rates that were measured in 2022 (Fig. 3g).

3.3 Drivers of NEP and Rff in 2015, 2018, and 2022

3.3.1 Comparison of drivers with long-term means for 2015, 2018, and 2022

Daily mean NEP for the growing seasons of 2015 and 2018 was mainly driven by daily mean incoming solar radiation (Rg), similar to the long-term daily mean of NEP for the period 2005–2022 (Fig. 4a). However, NEP during the 2022 growing season was more strongly driven by daily mean SWC than by Rg, as indicated by its high CVI (Fig. 4a). Daily mean Tair and VPD were the second-most important drivers of NEP in 2015 and 2018, with CVI values higher than those for the long-term mean from 2005–2022. In contrast to NEP, daily mean Rff for the growing seasons of 2019–2021 was mainly driven by daily mean SWC, followed by daily mean $Tair_{ff}$ and TS (Fig. 4b). We found that daily mean SWC was the main driver of Rff in 2018, with a much higher CVI compared to other years, followed by daily mean TS. Overall, the CVI for all variables was much lower in 2022 compared to other years (Fig. 4b).

3.3.2 Temporal development of important drivers of daytime NEP and daily Rff

Testing the temporal development of the main drivers of daytime NEP with SHAP analysis revealed that, overall, SWC, VPD, and Tair decreased NEP during all CSAD events (Fig. 5), while Rg increased daytime NEP. During the two CSAD events in 2015, both Tair and VPD were always asso-

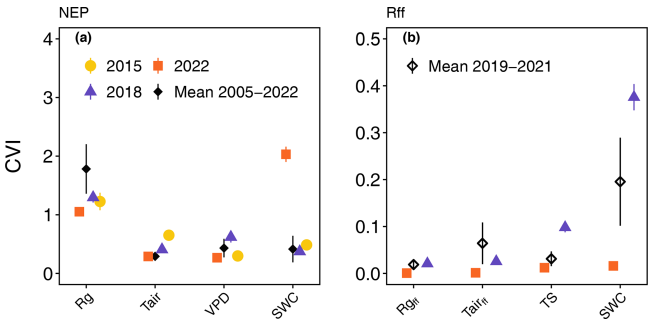

Figure 4. Driver analyses of daily mean **(a)** net ecosystem productivity (NEP) and **(b)** forest-floor respiration (Rff) during the growing seasons of 2015, 2018, and 2022, compared with the long-term daily mean NEP (2005–2022) and the long-term daily mean Rff (2019–2021), which were calculated for each year separately. Note that Rff was not measured in 2015. The effect of the driver (feature) variables is given by their conditional variable importance (CVI). Rg (incoming solar radiation), Tair (air temperature), VPD (vapour pressure deficit), and SWC (soil water content) were considered.

ciated with a decrease in NEP, while SWC exhibited a less consistent pattern, showing an increase in NEP during the first CSAD event and a decrease in NEP during the second (Fig. 5a). Nevertheless, the mean contributions of Tair, SWC, and VPD to NEP_{DT} during the CSAD events of 2015 were negative, with Tair having the largest effect on reducing NEP (Fig. 5a). As stated previously, Rg enhanced NEP_{DT} in both 2015 CSAD events, contributing positively to NEP (Fig. 5a). During the CSAD event of 2018, the mean contributions of Tair, VPD, and SWC to NEP_{DT} were also all negative, leading to a decrease in NEP (Fig. 5b). In contrast to 2015, SWC had the largest negative effect on daytime NEP during the 2018 CSAD event, although it had clear positive effects prior to the CSAD onset. Rg both enhanced and decreased NEP_{DT} during the CSAD event of 2018, which resulted in a small mean positive contribution (Fig. 5b). As observed in 2018, the mean contributions of Tair, VPD, and SWC were all negative during the CSAD event of 2022, leading to a decrease in NEP (Fig. 5c). As in 2018, prior to the 2022 CSAD event, SWC had a positive effect on daytime NEP; however, it then contributed the most to the decrease in NEP during the 2022 CSAD event. As observed previously, Rg also increased daytime NEP during the 2022 CSAD event, as shown by its positive contribution (Fig. 5c). Lastly, during the 2005–2022 reference period (from 7 July to 23 August), Tair, VPD, and SWC affected daytime NEP negatively, although the contributions of VPD and SWC were close to zero (Fig. 5d). In contrast, the mean contribution of Rg to NEP_{DT} was positive, resulting in an increase in NEP_{DT} during the 2005–2022 reference period (Fig. 5d).

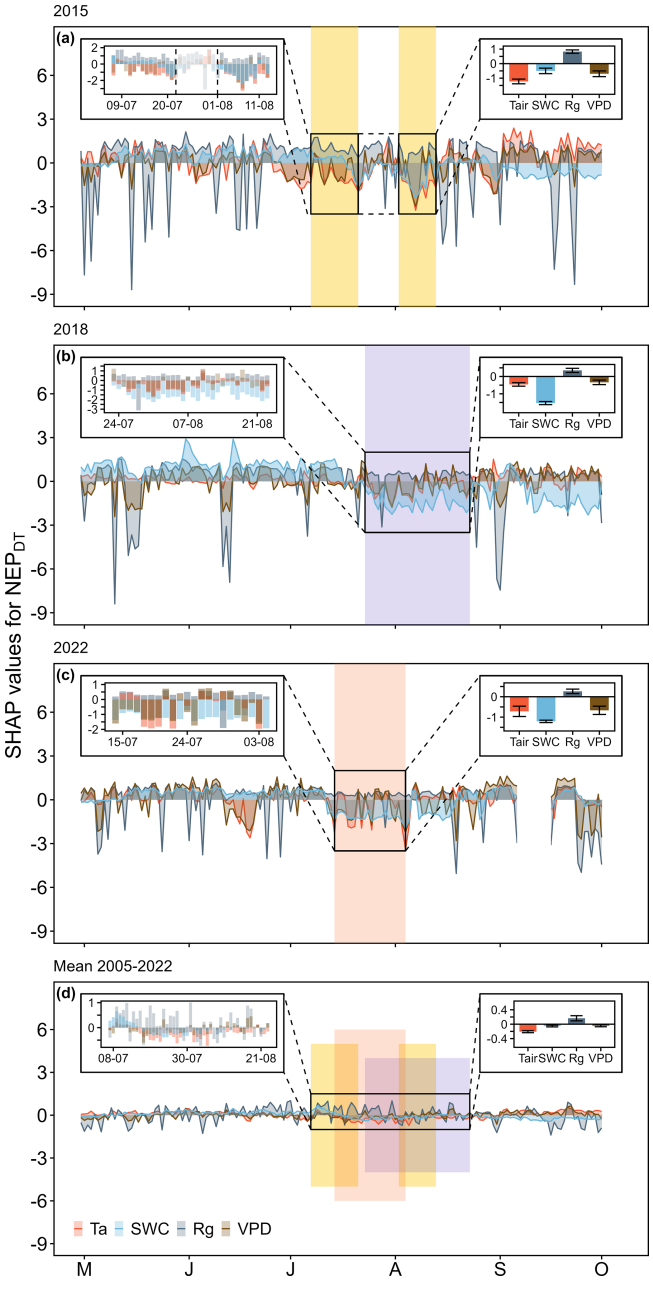

Figure 5. Temporal course of feature contributions to daytime mean net ecosystem productivity (NEP_{DT}) during the growing seasons of **(a)** 2015, **(b)** 2018, **(c)** and 2022, as well as with respect to **(d)** the long-term mean for the period 2005–2022 (indicated by SHAP values for Tair, incoming radiation (Rg), VPD, and SWC). The small insets on the left show the CSAD events **(a–c)** and the reference period for 2005–2022 **(d)**. The small insets on the right show the mean SHAP values (± SD) for Tair, SWC, Rg, and VPD during the CSAD events **(a–c)** and during the reference period for 2005–2022 **(d)**. Positive SHAP values indicate positive effects on the response variable NEP, while negative SHAP values indicate negative effects. Coloured areas show the periods during which CSAD events occurred in 2015, 2018, and 2022 **(a–c)**; they are also shown in panel **(d)** to highlight the reference period for the long-term mean (2005–2022).

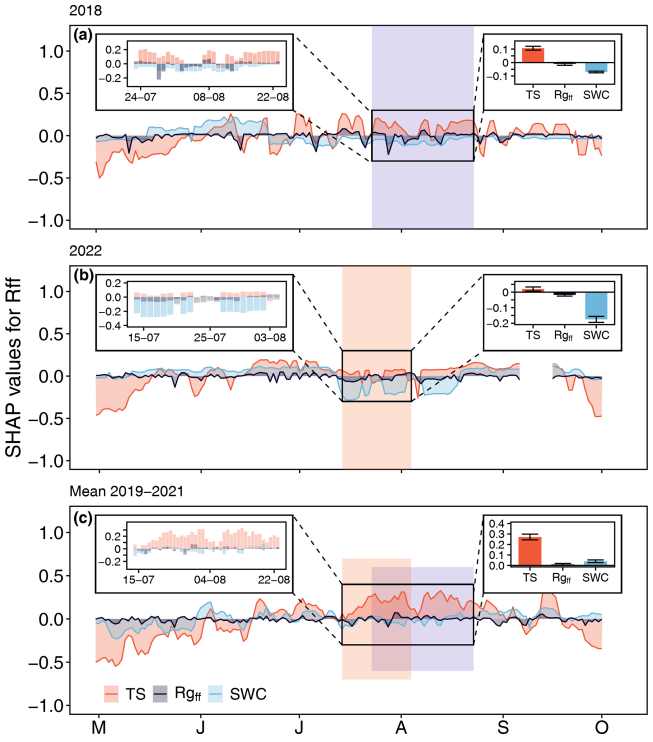

Figure 6. Temporal course of feature contributions to daily mean forest-floor respiration (Rff) during the growing seasons of **(a)** 2018 and **(b)** 2022, as well as during **(c)** the non-CSAD years for the period 2019–2021 (indicated by SHAP values for soil temperature (TS)), incoming radiation at the forest floor (Rg_{ff}), and SWC. The small insets on the left show the CSAD events **(a, b)** and the reference period for 2019–2021 (from 14 July to 23 August) **(d)**. The small insets on the right show mean SHAP values (± SD) for TS, Rg_{ff}, and SWC during the CSAD events **(a, b)** and during the reference period for 2019–2021 **(c)**. Positive SHAP values indicate a positive effect on the response variable Rff, while negative SHAP values indicate negative effects. Coloured areas show the periods during which CSAD events occurred; they are also shown in panel **(c)** to highlight the reference period for 2019–2021.

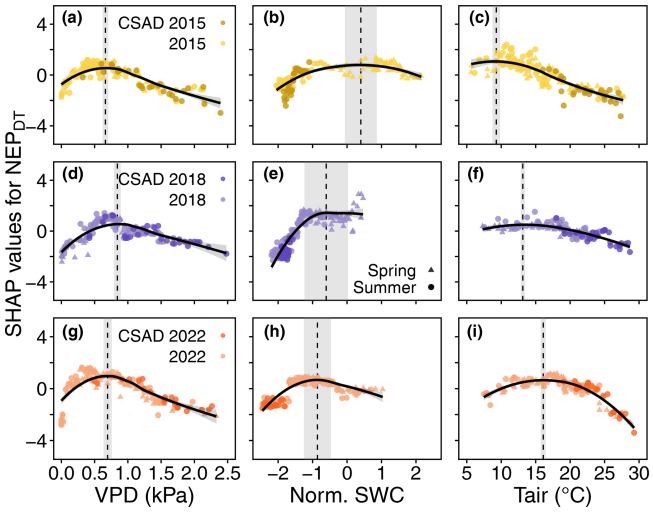

Figure 7. Detection of VPD, SWC, and Tair values corresponding to the maximum rate of daytime mean net ecosystem productivity (NEP_{DT}) during the growing seasons of 2015, 2018, and 2022. Positive (negative) SHAP values represent positive (negative) effects on NEP_{DT}. The vertical dashed lines and grey bands show VPD (**a**, **d**, **g**), SWC (**b**, **e**, **h**), and Tair (**c**, **f**, **i**), along with their standard deviations. These correspond to the largest effect on NEP_{DT}, based on the maximum marginal contribution of each driver in the SHAP analysis to NEP for the years 2015, 2018, and 2022.

In accordance with the previous analysis for NEP, the decrease in daily Rff during the 2018 and 2022 CSAD events was mainly driven by the negative effects of SWC (Fig. 6a and b). In contrast, TS increased Rff during both CSAD events, with much larger effects during the 2018 CSAD event than during the 2022 CSAD event. This coincided with negative effects of SWC on Rff starting in mid-June, i.e. 1 month prior to the 2018 CSAD event (Fig. 6a), while during the 2022 CSAD event, SWC effects only became negative shortly before the 2022 event (Fig. 6b). The effect of Rg_{ff} during the 2018 and 2022 CSAD events was positive but close to zero overall (Fig. 6a and b). For comparison, during the 2019–2021 reference period (from 14 July to 23 August), TS had the largest positive effect on Rff compared to the CSAD events in 2018 and 2022, which persisted typically until September, when senescence and leaf fall set in (Fig. 6c). On the other hand, the effects of Rg_{ff} and SWC varied around zero throughout all reference period summers (June, July, and August) (Fig. 6c). Overall, mean contributions to changes in Rff during the 2019–2021 reference period were dominated by the positive effects of TS and close-to-zero contributions of Rg_{ff} and SWC (Fig. 6c).

3.3.3 Driver thresholds with the largest effects on daytime mean NEP and daily mean Rff during the CSAD years

We derived thresholds for the drivers VPD, SWC, Tair, and TS to test if the absolute values of these drivers during the CSAD events actually differed from the absolute values that showed the largest effects on NEP_{DT} or Rff (based on the maximum marginal contributions from the SHAP analysis). Threshold values differed among the CSAD years, particularly for SWC_NEP_{max} and SWC_Rff_{max}, which were positive in 2015 and 2018 but negative in 2022 (Table 3). VPD_NEP_{max} was relatively low for all CSAD years (between 0.7 and 0.8 kPa), while $Tair\_NEP_{max}$ increased from around 10 °C in 2015 to 13 °C in 2018 and 16 °C in 2022. For comparison, TS_Rff_{max} was around 19 °C in 2018 and 15.6 °C in 2022. Comparing measured driver values to these thresholds revealed that most daytime mean VPD values during the CSAD events were typically higher than the respective VPD_NEP_{max} threshold for each of the CSAD years, reaching values of up to 2.5 kPa (Fig. 7a, d, and g), with

Table 3. Absolute driver thresholds (mean ± the standard error (SE)) associated with the largest effect on NEP_{DT} or Rff during the 3 CSAD years, along with the long-term means (2005–2022 for NEP and 2019–2021 for Rff). Identification was based on the maximum marginal contribution of each driver (VPD, SWC, Tair, and TS) in the SHAP analysis for each year.

Year	VPD_NEP_{max} (kPa)	SWC_NEP_{max} (normalized)	$Tair\_NEP_{max}$ (°C)	TS_Rff_{max} (°C)	SWC_Rff_{max} (normalized)
2015	0.66 ± 0.04	0.40 ± 0.43	9.79 ± 0.56	NA	NA
2018	0.84 ± 0.05	0.14 ± 0.6	13.13 ± 0.30	19.15 ± 0.07	0.58 ± 0.07
2022	0.77 ± 0.06	−0.86 ± 0.4	15.95 ± 0.37	15.60 ± 0.07	−0.73 ± 0.09

NA: not available.

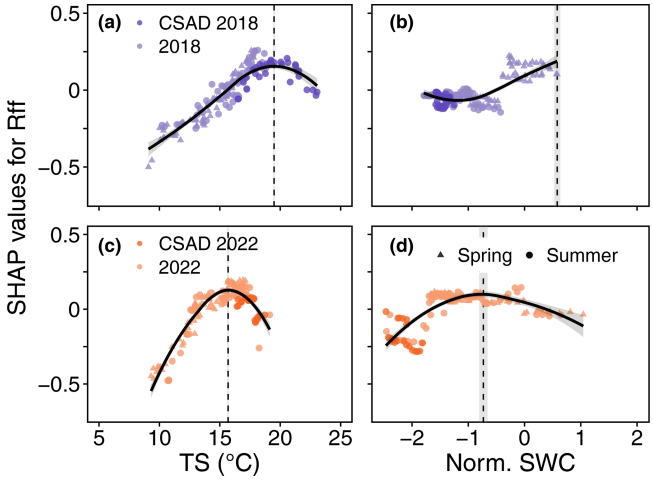

Figure 8. Detection of soil temperature (TS) and SWC values corresponding to the maximum rate of daily mean forest-floor respiration (Rff) in 2018 and 2022. Positive (negative) SHAP values represent positive (negative) effects on Rff. The vertical dashed lines and grey bands show TS **(a, c)** and SWC **(b, d)**, along with their standard deviations. These correspond to the largest effect on Rff, based on the maximum marginal contribution of each driver in the SHAP analysis to Rff for the years 2018 and 2022.

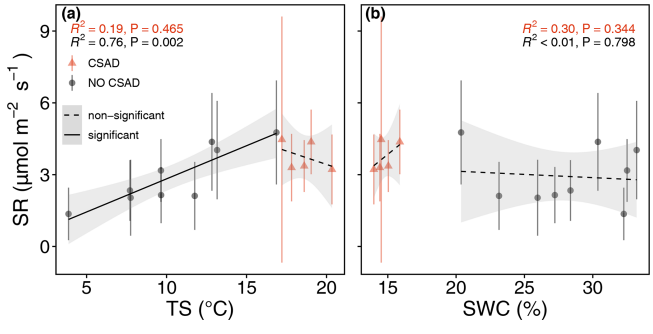

Figure 9. Linear relationships of daily mean soil respiration (SR) with **(a)** soil temperature (TS) and **(b)** soil water content (SWC) during the CSAD event of 2022 and for the rest of 2022. Two models were fitted separately for the periods with and without the CSAD event. The goodness of fit is expressed using R^2 and p values (P) in each panel, categorized according to a colour scale.

only a few exceptions. In contrast, all daytime mean SWC values measured during the CSAD events were far below the SWC_NEP_{max} thresholds for all CSAD years (Fig. 7b, e, and h), resulting in highly negative effects on daytime NEP. We also observed a decrease in SWC_NEP_{max} values from 2015 to 2022 (Fig. 7b, e, and h; Table 3). Likewise, daytime mean Tair measured during the CSAD events was far above the $Tair\_NEP_{max}$ threshold for all CSAD events (Fig. 7c, f, and i; Table 3). In addition, we observed an increase in $Tair\_NEP_{max}$ values from 2015 to 2022 (Fig. 7c, f, and i; Table 3). We also observed positive relationships between SWC_NEP_{max} and mean SWC, as well as between VPD_NEP_{max} and mean VPD, throughout the different growing seasons (Fig. A5). Applying the same analysis to daily mean Rff (Fig. 8) revealed that daily mean TS measured during the CSAD event in 2018 was around the TS_Rff_{max} threshold for that year (Fig. 8a), while measured TS values were higher than the TS_Rff_{max} threshold during the CSAD event in 2022 (Fig. 8b). As with NEP, SWC values measured during the CSAD events of 2018 and 2022 were far below their respective SWC_Rff_{max} thresholds (Fig. 8b and d), with the measured data and SWC_Rff_{max} thresholds being much lower in 2022 than in 2018 (Fig. 8b and d; Table 3).

3.4 SR responses to TS and SWC in 2022

As seen above, daily mean SR rates mirrored the responses of Rff (Fig. 3), albeit with a much coarser time resolution. The relationship between SR and TS, as well as that between SR and SWC, varied depending on whether CSAD events were considered or not (Fig. 9). When no CSAD event was recorded, daily mean SR significantly increased with TS ($R^2 = 0.76$; $P = 0.002$; linear regression). However, during the CSAD events, SR did not respond to TS ($R^2 = 0.19$; Fig. 9a). On the other hand, regardless of whether a CSAD event was recorded or not, SR did not respond to variations in SWC ($R^2 < 0.01$ and $R^2 = 0.3$, respectively; Fig. 9b).

4 Discussion

In this study, we identified three CSAD events over the last 18 years (i.e. 2015, 2018, and 2022) in a mixed deciduous

montane forest. Although these events were of comparable intensity, they differed in terms of timing. We further assessed the mainly negative impacts of these CSAD events on ecosystem CO_2 fluxes (NEP, GPP, and Reco) and forest-floor respiration (Rff). Moreover, we quantified the temporal contributions of the main drivers (VPD, Tair, Rg, SWC, and TS) to these fluxes during the CSAD events and the respective growing seasons. Pronounced differences in driver effects and their temporal development were found for ecosystem vs. forest-floor fluxes, as well as among drivers and CSAD events. In addition, we saw the first signs of the acclimation of NEP to such CSAD events, indicated by changes in the sensitivities of NEP to its drivers – both within the same growing season and among different growing seasons. This also suggests that predicting site-specific CSAD events and their impacts might become more challenging in the future.

4.1 CSAD events

Several recent studies have shown that Europe has already experienced (and will continue to experience) increased intensity and frequency of CSAD conditions in the future (e.g. Shekhar et al., 2024; Markonis et al., 2021). This increased occurrence of extremes was also evident during the 18 years (2005–2022) of eddy covariance measurements at CH-Lae, with 3 years (2015, 2018, and 2022) characterized by CSAD events within the last 8 years (2015–2022). Moreover, 2 other years, 2019 and 2020, were also characterized by atmospheric drought, albeit at a lower intensity than the 3 years identified here (Fig. 1). However, these years did not show co-occurring soil drought at our forest site and were therefore not classified as CSAD years. This nicely illustrates the importance of site-specific environmental conditions when discussing the impact of extreme compound events at larger spatial scales (Shekhar et al., 2024). Interestingly, even though the intensities of the CSAD events that occurred in 2015, 2018, and 2022 were comparable in terms of SWC and VPD values, the pre-conditions and timing of these events were different. Pre-conditions (pertaining to late spring or early summer) – especially those regarding soil moisture, temperature, or VPD – can be wet and cool, near to normal, or dry and warm. Thus, depending on these pre-conditions, the impact of any CSAD event on forest performance will differ, as shown here. Prior to a CSAD event, soil moisture plays a vital role in determining how well the forest can resist and recover from the stress of a CSAD event (Jiao et al., 2021). Dry and warm conditions, opposite to non-limiting ones before a CSAD event, can put the forest under additional water stress during the CSAD event, making it more susceptible to drought and heat stress (da Costa et al., 2018). However, even normal soil moisture and warm conditions in spring, which favour productivity but are also accompanied by increased water demands for evapotranspiration, can lead to increased soil drying. This, in turn, can amplify extreme dryness stress during summer droughts, as observed during the 2018 CSAD event at our mixed deciduous forest site (CH-Lae) and across Central Europe (Gharun et al., 2020; Bastos et al., 2020; Shekhar et al., 2020). Thus, CSAD events will require our full attention in the future since their impacts strongly differ depending not only on their frequency, duration, and intensity but also on prior site-specific environmental conditions experienced by the ecosystem.

4.2 Forest CO_2 fluxes and their respective drivers

4.2.1 Net ecosystem productivity (NEP)

The CSAD events of 2015, 2018, and 2022 resulted in a significant decrease in NEP, largely due to decreasing GPP (between 16 % and 28 %), while ecosystem respiration (Reco) either decreased or remained unchanged compared to the long-term mean at the mixed deciduous forest site. Such reductions in GPP during CSAD events have been observed in earlier studies, particularly those focused on beech species, the dominant species at our forest site (Ciais et al., 2005; Bastos et al., 2020; Dannenberg et al., 2022; D'Orangeville et al., 2018; Xu et al., 2020; Gharun et al., 2020). Increased stomatal closure in response to high VPD and low soil moisture (i.e. stomatal response), reductions in photosynthesis due to a reduced carboxylation rate (Rubisco activity) at high temperatures (i.e. non-stomatal response; Buckley, 2019; Gourlez de la Motte et al., 2020) at the leaf level, and reduced canopy conductance at the ecosystem level (Ciais et al., 2005; Granier et al., 2007; Gharun et al., 2020) are typically associated with such CSAD events.

Our driver analysis revealed that, among the considered features, air temperature had the largest effect on reducing NEP_{DT} during the CSAD event in 2015; however, this was not the case in the other years, suggesting that stomatal responses to GPP were generally more relevant than temperature-related non-stomatal responses (Granier et al., 2007). Moreover, the major drivers we identified, i.e. VPD and SWC, support stomatal responses as underlying mechanisms for the reduction in net CO_2 uptake via GPP (Dannenberg et al., 2022; Fu et al., 2022; Petek-Petrik et al., 2023; van der Woude et al., 2023) during the CSAD events in 2015, 2018, and 2022. However, the contributions of these dryness-related variables varied among the CSAD events, suggesting that the response of the forest differed depending on the intensity of soil dryness (SWC) and air dryness (VPD) during the CSAD events. Also, conditions prior to the CSAD event seemed to play an important role as SWC was more important for NEP during the 2022 CSAD event, which followed a period of prevailing soil drought, compared to the 2015 and 2018 CSAD events.

Another line of argumentation regarding dryness-related vs. temperature-related drivers of reduced NEP during CSAD events involves Reco, which comprises two major components – plant and soil respiration. In our study, Reco was 7 %–31 % lower during the 3 CSAD years compared to

the other years, supporting the argument for dryness-related over temperature-related drivers. While plant respiration typically increases in response to high temperatures (Schulze et al., 2019), it also depends on the intensity of the event. If substrate (i.e. carbohydrate) availability is diminished during a CSAD event due to reduced GPP, respiration can also decrease (Janssens et al., 2001; Ciais et al., 2005; Von Buttlar et al., 2018), albeit typically to a lesser extent than GPP (Schwalm et al., 2010). Similarly, soil respiration decreases when the substrate supply for root and microbial respiration is low (Högberg et al., 2001; Ruehr et al., 2009). Moreover, soil respiration is known to be minimal when soil moisture is low (due to reduced microbial and root respiration) during CSAD events (Ruehr et al., 2010; Von Buttlar et al., 2018; Wang et al., 2014), as observed at our site in 2022. In addition to the standard response of NEP (and its components GPP and Reco) to abiotic drivers (VPD, SWC, and Tair), NEP sensitivity to these drivers can vary from one growing season to another (Grossman, 2023), especially during drought conditions, indicating the acclimation of NEP (Crous et al., 2022; Aspinwall et al., 2017; Sendall et al., 2015; Sperlich et al., 2019). This variation in NEP sensitivity to VPD, SWC, and Tair during the 2015, 2018, and 2022 growing seasons was clearly observed in our study (see the response curves in Fig. 7). The thresholds derived from the response curves illustrating SHAP values vs. abiotic drivers (Fig. 7) indicated an acclimation of NEP to higher VPD (in 2018 and 2022) and to lower SWC (in 2022). We observed a shift towards drier conditions in VPD and SWC values corresponding to the maximum marginal contributions of these features to NEP_{DT} during the CSAD years (Fig. 7 and A5). Such instances of drought acclimation could be due to biophysical adjustments, such as access to soil water from deeper soil layers (Brinkmann et al., 2019), changes in photosynthetic thermal acclimation, and changes in stomatal sensitivity to VPD (Aspinwall et al., 2017; Smith and Dukes, 2017; Gessler et al., 2020). This acclimation of NEP to higher VPD and lower SWC will be critical in the future, enabling forests to persist (longer) during CSAD events (Kumarathunge et al., 2019).

4.2.2 Forest-floor respiration (Rff) and soil respiration (SR)

The CSAD event of 2022 led to a more pronounced and rapid decrease in Rff compared to the CSAD event of 2018, resulting in smaller CO_2 losses at the forest floor compared to the 2018 CSAD event and the 2019–2021 reference period. We observed a similar seasonal trend in Rff and SR, but SR was consistently higher than Rff (Fig. 3d). Rff comprises both soil and understory vegetation respiration. At CH-Lae, the understory LAI (leaf area index) decreased in late spring (Paul-Limoges, 2017) as trees leafed out, thereby reducing light reaching the forest floor. Thus, during the growing season, the majority of the respiratory CO_2 fluxes from below the canopy are attributed to SR. However, a small portion of SR can be offset by photosynthesis from vegetation still growing below the canopy (e.g. seedlings of *Fagus sylvatica* and other herbaceous plants). Given that GPP_{ff} remained at zero during the growing seasons (Fig. A6), we assumed that the effect of photosynthesis on daily Rff is negligible. European mixed forests are usually more resistant to drought than monospecific forests in terms of microbial soil respiration (Gillespie et al., 2020). For example, Gillespie et al. (2020) found that CO_2 emissions did not decrease under drought conditions in natural mixed European forests. However, a reduction in SR during drought periods has been widely reported in other studies (e.g. Ruehr et al., 2010; Schindlbacher et al., 2012; Wang et al., 2014; Sun et al., 2019). Nevertheless, the interplay of intensity, duration, and biotic components can trigger various responses of the forest floor in the different ecosystems (Talmon et al., 2011; Jiao et al., 2021).

The decreased importance of TS during the CSAD events of 2018 and 2022, compared to the 2019–2021 reference period (Fig. 6), was driven by limitations in Rff and SR caused by SWC. In accordance with the SR analysis, we found no effect of TS during the CSAD event of 2022 (Fig. 9). Drought periods in forests can indeed diminish the temperature sensitivity of SR (Jassal et al., 2008; Ruehr et al., 2010; Sun et al., 2019; Schindlbacher et al., 2012; van Straaten et al., 2011; Wang et al., 2014). Generally, SWC is not limiting at CH-Lae, but exceptions can occur during summer (Knohl et al., 2008; Ruehr et al., 2010; Zomer et al., 2022). We know that SR comprises both heterotrophic and autotrophic respiration (Ruehr and Buchmann, 2009; Wang et al., 2014; Zheng et al., 2021). A large component of heterotrophic respiration is microbial activity in the soil. Under drought conditions, microbial activity is typically reduced by the limited diffusion of soluble carbon substrate for extracellular enzymes (Manzoni et al., 2012). Consequently, litter decomposition rates also decrease (Deng et al., 2021). If decomposition rates decrease, soil organic matter increases, resulting in higher C and N levels in the soil (van der Molen et al., 2011). At the same time, drought reduces photosynthesis, meaning plants tend to keep non-structural carbohydrates in leaves or roots to sustain living tissues (Högberg et al., 2008). As a result, root activity and production are downregulated (Deng et al., 2021), which can lead to a decoupling of photosynthetic and underground activities (Ruehr et al., 2009; Barba et al., 2018). Eventually, soil drought can significantly alter the N and C cycles in the ecosystem (Deng et al., 2021; Bogati and Walczak, 2022).

The TS and SWC levels at which Rff_{max} was observed varied from growing season to growing season, as seen in 2018 and 2022 (Fig. 8). SWC levels recorded during the CSAD events was clearly below SWC_Rff_{max} levels, whereas TS recorded during the CSAD events was observed to be within the range of TS_Rff_{max} in 2018. The interplay and seasonal trends of TS and SWC can thus determine the abiotic conditions under which the highest respiration rate is found. Even though SR is projected to increase with global warming

(Schindlbacher et al., 2012), the more frequent occurrence of droughts (Grillakis, 2019) could partially offset these emissions (Zheng et al., 2021), as observed in the decrease in Rff during CSAD events. However, the decrease in CO_2 emissions can be compensated for by CO_2 bursts from rain events occurring after drought periods (Lee et al., 2002), as observed after the CSAD event in 2022 (Fig. 3d). In general, a recovery of SR is expected if soil moisture quickly returns to normal conditions (Yao et al., 2023). Yet, biotic factors, such as fine roots, are crucial for tree recovery after drought periods (Netzer et al., 2016; Hikino et al., 2022a, b). For example, it is well known that the fine roots of *Fagus sylvatica* can grow to deeper soil depths during drought periods. However, this is only the case when the drought is not too severe; otherwise, they may be shed (Hildebrandt, 2020). Indeed, Nickel et al. (2018) found a progressive decrease in vital fine roots after repeated droughts in a mixed deciduous forest in Europe. Hence, the pre- and post-conditions, timing, intensity, and duration of a CSAD event are very important for predicting consequences in terms of respiratory CO_2 emissions.

5 Conclusions

For our mixed deciduous forest, we found initial signs of NEP acclimation to more extreme soil-drought (low SWC) and atmospheric-drought conditions (high VPD) when comparing NEP sensitivities to these drivers during the same growing season. This acclimation will be fundamental for drought resistance in the future. Nevertheless, we expect to witness a larger reduction in GPP with increasingly extreme CSAD events in the future, even if this is complemented by a reduction in Reco. Hence, responses to CSAD events might lead to a reduction in the CO_2 sink capacity of the forest in the future. The study also highlighted the different behaviours of the responses of the above-canopy and forest-floor CO_2 fluxes during CSAD events. With further global warming in Europe, we expect an increase in Rff. However, with more extreme droughts and increasingly intense precipitation events, we expect a higher variability in CO_2 emissions from forest soils and thus uncertain consequences for soil carbon stocks. Ultimately, the consequences of CSAD events will influence the annual carbon budget of forests, potentially jeopardizing many restoration and reforestation projects or nature-based solutions proposed in the Paris Agreement.

Appendix A

Table A1. List of the instruments, models, and manufacturers used in this study.

Instrument	Model	Manufacturer
Infrared gas analyser (IRGA)[1]	LI-7500 (2004–2015)	LI-COR, Inc., Lincoln, NE, USA
Infrared gas analyser (IRGA)[1]	LI-7200 (2016–2022)	LI-COR, Inc., Lincoln, NE, USA
3D sonic anemometer[1]	HS-50	Gill Instruments Ltd., Lymington, UK
Air temperature and relative humidity[2]	Rotronic MP101A	Rotronic AG, Bassersdorf, Switzerland
Incoming radiation[2]	BF2	Delta-T Devices Ltd., Cambridge, UK
Infrared gas analyser (IRGA)[3]	LI-7500	LI-COR, Inc., Lincoln, NE, USA
3D sonic anemometer[3]	R-350	Gill Instruments Ltd., Lymington, UK
Air temperature and relative humidity[4]	CS215	Campbell Scientific Ltd., USA
Soil temperature and water content[5]	Decagon ECH2O EC-20 probes (2004–2020)	Pullman, WA, USA
Soil temperature and water content[5]	TEROS 12	METER Group, Inc., NE, USA
Incoming radiation[4]	LI190SB-L	LI-COR, Inc., Lincoln, NE, USA
Infrared gas analyser (IRGA)[6]	LI-8100	LI-COR, Inc., Lincoln, NE, USA
Soil temperature[6]	GTH 175/PT	GHM Messtechnik GmbH, Regenstauf, Germany
Soil water content[6]	HH2 Moisture Meter	Delta-T Devices Ltd., Cambridge, UK

[1] Above-canopy EC system (47 m height). [2] Above-canopy meteorological measurements (54 m height). [3] Below-canopy EC system (1.5 m height). [4] Below-canopy meteorological station (2 m height). [5] Forest-floor meteorological station (profile measurements at depths of 5, 10, 20, 30, and 50 cm), [6] Portable sensors (SR survey measurements).

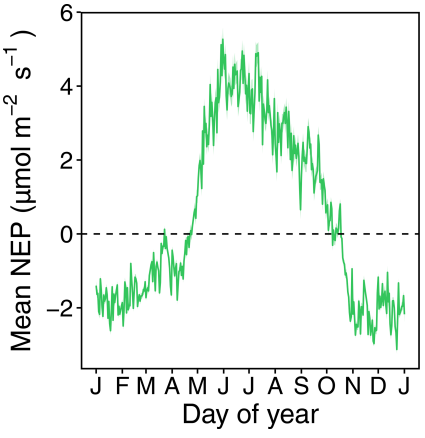

Figure A1. Long-term (2005–2022) daily means and standard deviations of net ecosystem productivity (NEP) at CH-Lae. The zero line indicates whether daily NEP is positive or negative. The growing season was identified as the period in which daily NEP was positive (1 May to 31 September). The x axis shows the months of the year.

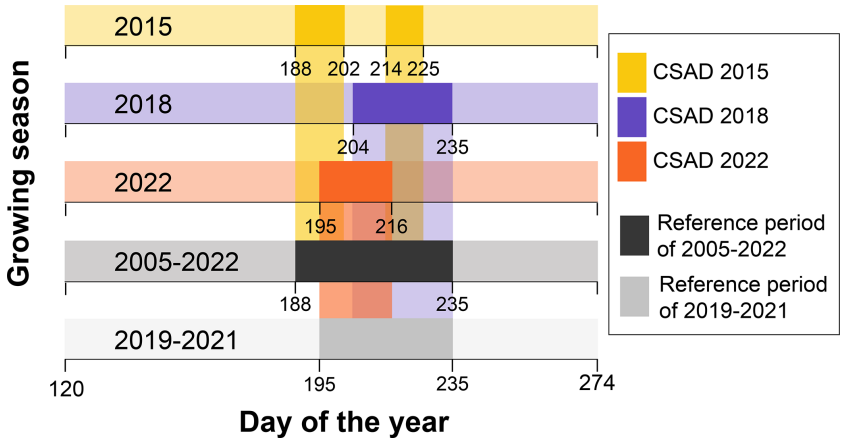

Figure A2. Graphical representations of the reference periods. The five horizontal bars display the three growing seasons with a CSAD event and the two long-term means, which are used as reference periods for comparison (2005–2022 for ecosystem-level measurements and 2019–2021 for forest-floor measurements). The CSAD periods are marked for each growing season in the CSAD years. The reference period for the 2005–2022 mean used in our analyses corresponds to the interval of time between day 188 (7 July) and day 235 (23 August), while the reference period for the 2019–2021 mean corresponds to the interval of time between day 195 (14 July) and day 235 (23 August).

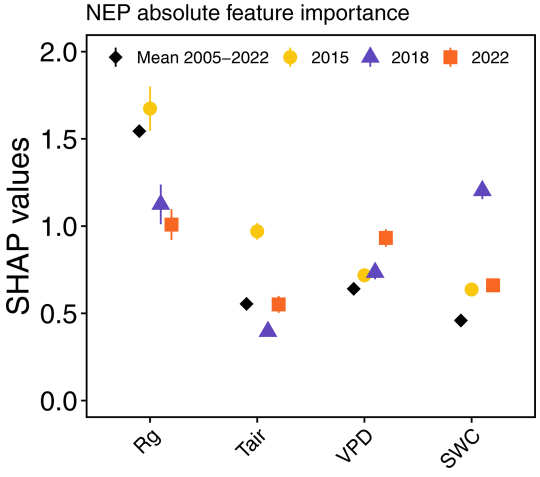

Figure A3. Absolute mean SHAP values (± SE) for daily mean NEP, obtained using the "xgboost" model.

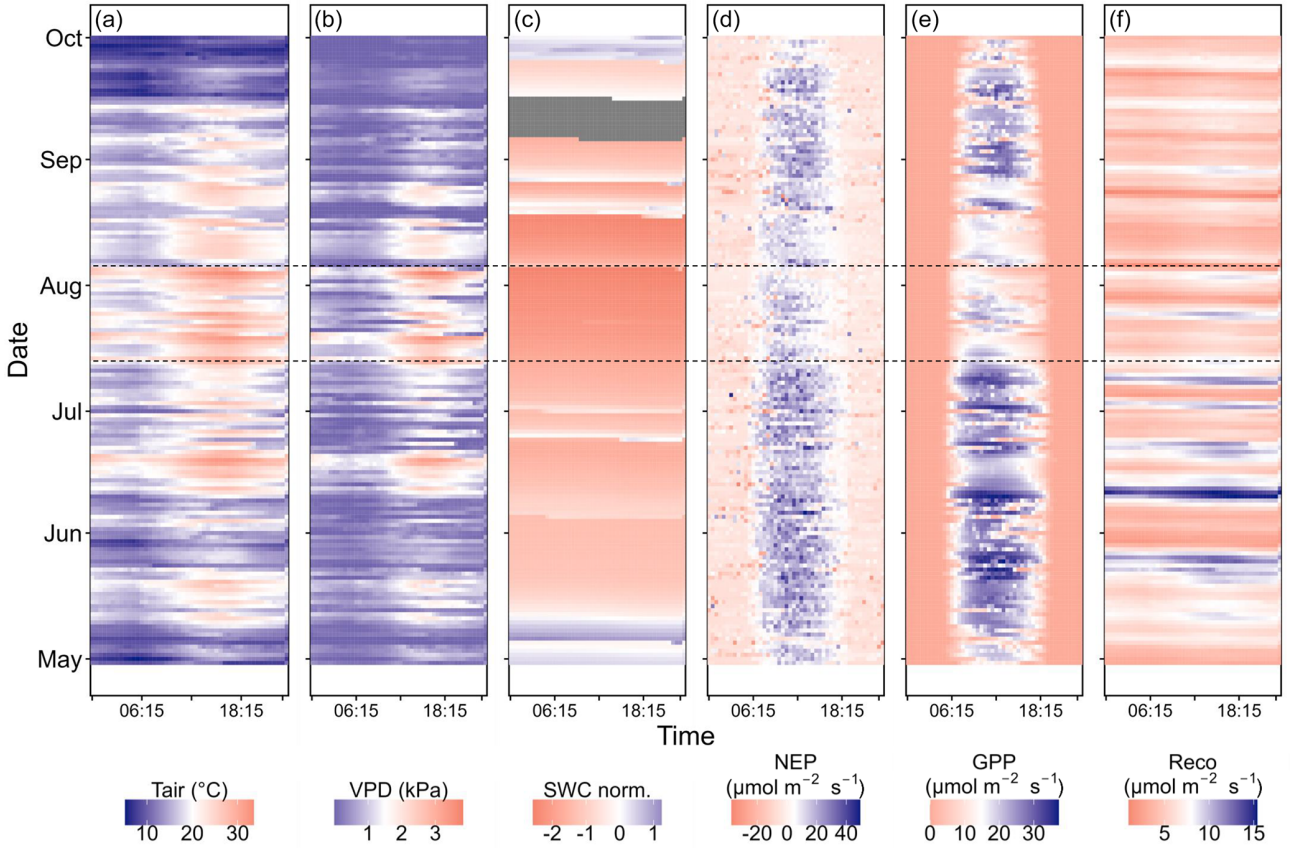

Figure A4. Diurnal variation (x axis) and intra-annual variation (y axis) in **(a)** air temperature (Tair), **(b)** VPD, **(c)** normalized soil water content (SWC at 20 cm depth), **(d)** net ecosystem productivity (NEP), **(e)** gross primary productivity (GPP), and **(f)** ecosystem respiration (Reco) during the 2022 growing season; 30 min averages are plotted in all panels. The two dashed black lines (corresponding to 14 July 2022 and 4 August 2022) mark the CSAD event that occurred in the summer of 2022.

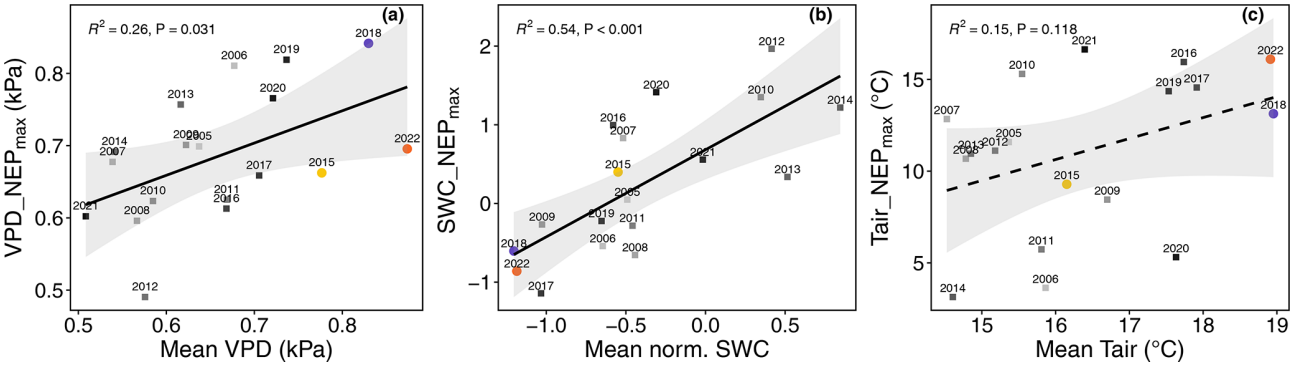

Figure A5. Linear regressions of mean VPD, SWC, and Tair values during the growing season of a given year against the maximum marginal contributions of VPD, SWC, and Tair (abbreviated as feature_NEP_{max}) to daytime NEP. SWC values are normalized. The grey bands around the regression lines each indicate the 95 % confidence interval. R^2 and p values are given as well.

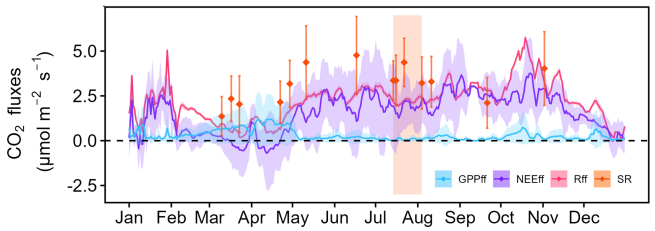

Figure A6. Forest-floor CO_2 fluxes in 2022. The continuous lines show gap-filled and partitioned daily mean fluxes, as well as standard deviations (coloured bands); 30 min averages are plotted. The diamonds represent daily means of manual soil respiration measurements; standard deviations are given as well. The area coloured in orange represents the CSAD event of 2022.

Data availability. The R scripts used for the data analyses and plots are available upon request from the corresponding author. The data are available in the following repositories: https://doi.org/10.3929/ethz-b-000687324 (Scapucci et al., 2024) and https://doi.org/10.3929/ethz-b-000582198 (Shekhar et al., 2022).

Author contributions. LS, AS, MG, and NB: conceptualization of the study. LS, AS, SAB, and AB: field campaigns. LS, AS, and LH: data processing and management. LS and AS: data analyses. LS, AS, and NB: paper writing. All authors: revision and editing of the paper.

Competing interests. The contact author has declared that none of the authors has any competing interests.

Disclaimer. Publisher's note: Copernicus Publications remains neutral with regard to jurisdictional claims made in the text, published maps, institutional affiliations, or any other geographical representation in this paper. While Copernicus Publications makes every effort to include appropriate place names, the final responsibility lies with the authors.

Acknowledgements. The authors acknowledge and appreciate the great support from members of the Grassland Sciences Group, especially Anna Katarina Gilgen, Luana Krebs, Julia Hauri, Franziska Richter, Yi Wang, Fabio Turco, Ruikun Gou, Roland Anton Werner, and Davide Andreatta.

Financial support. This research has been supported by the ETH Zürich project FEVER (grant no. ETH-27 19-1) and the SNF-funded projects COCO (grant no. 200021_197357), ICOS-CH Phase 3 (grant no. 20F120_198227), and EcoDrive (grant no. IZCOZ0_198094).

Review statement. This paper was edited by Andrew Feldman and reviewed by Peter Petrík and one anonymous referee.

References

Anderegg, W. R. L., Wu, C., Acil, N., Carvalhais, N., Pugh, T. A. M., Sadler, J. P., and Seidl, R.: A climate risk analysis of Earth's forests in the 21st century, Science, 377, 1099–1103, https://doi.org/10.1126/science.abp9723, 2022.

Aspinwall, M. J., Vårhammar, A., Blackman, C. J., Tjoelker, M. G., Ahrens, C., Byrne, M., Tissue, D. T., and Rymer, P. D.: Adaptation and acclimation both influence photosynthetic and respiratory temperature responses in, Tree Physiol., 37, 1095–1112, https://doi.org/10.1093/treephys/tpx047, 2017.

Aubinet, M., Vesala, T., and Papale, D.: Eddy covariance: a practical guide to measurement and data analysis, Springer Science & Business Media, https://doi.org/10.1007/978-94-007-2351-1, 2012.

Barba, J., Lloret, F., Poyatos, R., Molowny-Horas, R., and Yuste, J. C.: Multi-temporal influence of vegetation on soil respiration in a drought-affected forest, Iforest, 11, 189–198, https://doi.org/10.3832/ifor2448-011, 2018.

Bastos, A., Ciais, P., Friedlingstein, P., Sitch, S., Pongratz, J., Fan, L., Wigneron, J. P., Weber, U., Reichstein, M., Fu, Z., Anthoni, P., Arneth, A., Haverd, V., Jain, A. K., Joetzjer, E., Knauer, J., Lienert, S., Loughran, T., McGuire, P. C., Tian, H., Viovy, N., and Zaehle, S.: Direct and seasonal legacy effects of the 2018 heat wave and drought on European ecosystem productivity, Science Advances, 6, eaba2724, https://doi.org/10.1126/sciadv.aba2724, 2020.

Birami, B., Gattmann, M., Heyer, A. G., Grote, R., Arneth, A., and Ruehr, N. K.: Heat Waves Alter Carbon Allocation and Increase Mortality of Aleppo Pine Under Dry Conditions, Frontiers in Forests and Global Change, 1, 8, https://doi.org/10.3389/ffgc.2018.00008, 2018.

Bogati, K. and Walczak, M.: The Impact of Drought Stress on Soil Microbial Community, Enzyme Activities and Plants, Agronomy-Basel, 12, 189, https://doi.org/10.3390/agronomy12010189, 2022.

Breiman, L.: Random forests, Mach. Learn., 45, 5–32, https://doi.org/10.1023/A:1010933404324, 2001.

Brinkmann, N., Eugster, W., Buchmann, N., and Kahmen, A.: Species-specific differences in water uptake depth of mature temperate trees vary with water availability in the soil, Plant Biol., 21, 71–81, https://doi.org/10.1111/plb.12907, 2019.

Buckley, T. N.: How do stomata respond to water status?, New Phytol., 224, 21–36, https://doi.org/10.1111/nph.15899, 2019.

Chen, T. and Guestrin, C.: XGBoost: A Scalable Tree Boosting System, in: Proceedings of the 22nd ACM SIGKDD International Conference on Knowledge Discovery and Data Mining, San Francisco, California, USA, https://doi.org/10.1145/2939672.2939785, 2016.

Chi, J. S., Zhao, P., Klosterhalfen, A., Jocher, G., Kljun, N., Nilsson, M. B., and Peichl, M.: Forest floor fluxes drive differences in the carbon balance of contrasting boreal forest stands, Agr. Forest Meteorol., 306, 108454, https://doi.org/10.1016/j.agrformet.2021.108454, 2021.

Ciais, P., Reichstein, M., Viovy, N., Granier, A., Ogée, J., Allard, V., Aubinet, M., Buchmann, N., Bernhofer, C., Carrara, A., Chevallier, F., De Noblet, N., Friend, A. D., Friedlingstein, P., Grünwald, T., Heinesch, B., Keronen, P., Knohl, A., Krinner, G., Loustau, D., Manca, G., Matteucci, G., Miglietta, F., Ourcival, J. M., Papale, D., Pilegaard, K., Rambal, S., Seufert, G., Soussana, J. F., Sanz, M. J., Schulze, E. D., Vesala, T., and Valentini, R.: Europe-wide reduction in primary productivity caused by the heat and drought in 2003, Nature, 437, 529–533, https://doi.org/10.1038/nature03972, 2005.

Copernicus Climate Change Service (C3S): European State of the Climate 2022, https://climate.copernicus.eu/esotc/2022 (last access: 26 January 2024), 2023.

Crous, K. Y., Uddling, J., and De Kauwe, M. G.: Temperature responses of photosynthesis and respiration in evergreen trees from boreal to tropical latitudes, New Phytol., 234, 353–374, https://doi.org/10.1111/nph.17951, 2022.

da Costa, A. C. L., Rowland, L., Oliveira, R. S., Oliveira, A. A. R., Binks, O. J., Salmon, Y., Vasconcelos, S. S., Junior, J. A. S., Ferreira, L. V., Poyatos, R., Mencuccini, M., and Meir, P.: Stand dynamics modulate water cycling and mortality risk in droughted tropical forest, Glob. Change Biol., 24, 249–258, https://doi.org/10.1111/gcb.13851, 2018.

Dannenberg, M. P., Yan, D., Barnes, M. L., Smith, W. K., Johnston, M. R., Scott, R. L., Biederman, J. A., Knowles, J. F., Wang, X., Duman, T., Litvak, M. E., Kimball, J. S., Williams, A. P., and Zhang, Y.: Exceptional heat and atmospheric dryness amplified losses of primary production during the 2020 U. S. Southwest hot drought, Glob. Change Biol., 28, 4794–4806, https://doi.org/10.1111/gcb.16214, 2022.

de la Motte, L. G., Beauclaire, Q., Heinesch, B., Cuntz, M., Foltynová, L., Sigut, L., Kowalska, N., Manca, G., Ballarin, I. G., Vincke, C., Roland, M., Ibrom, A., Lousteau, D., Siebicke, L., Neiryink, J., and Longdoz, B.: Non-stomatal processes reduce gross primary productivity in temperate forest ecosystems during severe edaphic drought, Philos. T. R. Soc. B, 375, 1810, https://doi.org/10.1098/rstb.2019.0527, 2020.

Deng, L., Peng, C. H., Kim, D. G., Li, J. W., Liu, Y. L., Hai, X. Y., Liu, Q. Y., Huang, C. B., Shangguan, Z. P., and Kuzyakov, Y.: Drought effects on soil carbon and nitrogen dynamics in global natural ecosystems, Earth-Sci. Rev., 214, 103501, https://doi.org/10.1016/j.earscirev.2020.103501, 2021.

Dirmeyer, P. A., Balsamo, G., Blyth, E. M., Morrison, R., and Cooper, H. M.: Land-atmosphere interactions exacerbated the drought and heatwave over northern Europe during summer 2018, AGU Advances, 2, e2020AV000283, https://doi.org/10.1029/2020AV000283, 2021.

D'Orangeville, L., Maxwell, J., Kneeshaw, D., Pederson, N., Duchesne, L., Logan, T., Houle, D., Arseneault, D., Beier, C. M., Bishop, D. A., Druckenbrod, D., Fraver, S., Girard, F., Halman, J., Hansen, C., Hart, J. L., Hartmann, H., Kaye, M., Leblanc, D., Manzoni, S., Ouimet, R., Rayback, S., Rollinson, C. R., and Phillips, R. P.: Drought timing and local climate determine the sensitivity of eastern temperate forests to drought, Glob. Change Biol., 24, 2339–2351, https://doi.org/10.1111/gcb.14096, 2018.

Fan, S. M., Wofsy, S. C., Bakwin, P. S., Jacob, D. J., and Fitzjarrald, D. R.: Atmosphere-biosphere exchange of CO_2 and O_3 in the Central-Amazon-Forest, J. Geophys. Res.-Atmos., 95, 16851–16864, https://doi.org/10.1029/JD095iD10p16851, 1990.

Fratini, G., Ibrom, A., Arriga, N., Burba, G., and Papale, D.: Relative humidity effects on water vapour fluxes measured with closed-path eddy-covariance systems with short sampling lines, Agr. Forest Meteorol., 166, 234–234, https://doi.org/10.1016/j.agrformet.2012.10.013, 2012.

Fu, Z., Ciais, P., Feldman, A. F., Gentine, P., Makowski, D., Prentice, I. C., Stoy, P. C., Bastos, A., and Wigneron, J.-P.: Critical soil moisture thresholds of plant water stress in terrestrial ecosystems, Sci. Adv., 8, eabq7827, https://doi.org/10.1126/sciadv.abq7827, 2022.

Gazol, A. and Camarero, J. J.: Compound climate events increase tree drought mortality across European forests, Sci. Total Environ., 816, 151604, https://doi.org/10.1016/j.scitotenv.2021.151604, 2022.

George, J. P., Bürkner, P. C., Sanders, T. G. M., Neumann, M., Cammalleri, C., Vogt, J. V., and Lang, M.: Long-term forest monitoring reveals constant mortality rise in European forests, Plant Biol., 24, 1108–1119, https://doi.org/10.1111/plb.13469, 2022.

Gessler, A., Bottero, A., Marshall, J., and Arend, M.: The way back: recovery of trees from drought and its implication for acclimation, New Phytol., 228, 1704–1709, https://doi.org/10.1111/nph.16703, 2020.

Gharun, M., Hörtnagl, L., Paul-Limoges, E., Ghiasi, S., Feigenwinter, I., Burri, S., Marquardt, K., Etzold, S., Zweifel, R., Eugster, W., and Buchmann, N.: Physiological response of Swiss ecosystems to 2018 drought across plant types and elevation, Philos. T. R. Soc. B, 375, 20190521, https://doi.org/10.1098/rstb.2019.0521, 2020.

Gillespie, L. M., Fromin, N., Milcu, A., Buatois, B., Pontoizeau, C., and Hättenschwiler, S.: Higher tree diversity increases soil microbial resistance to drought, Communications Biology, 3, 377, https://doi.org/10.1038/s42003-020-1112-0, 2020.

Gou, R., Buchmann, N., Chi, J., Luo, Y., Mo, L., Shekhar, A., Feigenwinter, I., Hörtnagl, L., Lu, W., and Cui, X.: Temporal variations of carbon and water fluxes in a subtropical mangrove forest: Insights from a decade-long eddy covariance measurement, Agr. Forest Meteorol., 343, 109764, https://doi.org/10.1016/j.agrformet.2023.109764, 2023.

Granier, A., Reichstein, M., Bréda, N., Janssens, I., Falge, E., Ciais, P., Grünwald, T., Aubinet, M., Berbigier, P., and Bernhofer, C.: Evidence for soil water control on carbon and water dynamics in European forests during the extremely dry year: 2003, Agr. Forest Meteorol., 143, 123–145, https://doi.org/10.1016/j.agrformet.2006.12.004, 2007.

Greco, S. and Baldocchi, D. D.: Seasonal variations of CO_2 and water vapour exchange rates over a temperate deciduous forest, Glob. Change Biol., 2, 183–197, https://doi.org/10.1111/j.1365-2486.1996.tb00071.x, 1996.

Grillakis, M. G.: Increase in severe and extreme soil moisture droughts for Europe under climate change, Sci. Total Environ., 660, 1245–1255, https://doi.org/10.1016/j.scitotenv.2019.01.001, 2019.

Grossiord, C., Sevanto, S., Borrego, I., Chan, A. M., Collins, A. D., Dickman, L. T., Hudson, P. J., McBranch, N., Michaletz, S. T., Pockman, W. T., Ryan, M., Vilagrosa, A., and McDowell, N. G.: Tree water dynamics in a drying and warming world, Plant Cell Environ., 40, 1861–1873, https://doi.org/10.1111/pce.12991, 2017.

Grossiord, C., Buckley, T. N., Cernusak, L. A., Novick, K. A., Poulter, B., Siegwolf, R. T. W., Sperry, J. S., and McDowell, N. G.: Plant responses to rising vapor pressure deficit, New Phytol., 226, 1550–1566, https://doi.org/10.1111/nph.16485, 2020.

Grossman, J. J.: Phenological physiology: seasonal patterns of plant stress tolerance in a changing climate, New Phytol., 237, 1508–1524, 2023.

Haberstroh, S., Werner, C., Grün, M., Kreuzwieser, J., Seifert, T., Schindler, D., and Christen, A.: Central European 2018 hot drought shifts scots pine forest to its tipping point, Plant Biol., 24, 1186–1197, https://doi.org/10.1111/plb.13455, 2022.

Harris, N. L., Gibbs, D. A., Baccini, A., Birdsey, R. A., de Bruin, S., Farina, M., Fatoyinbo, L., Hansen, M. C., Herold, M., Houghton, R. A., Potapov, P. V., Suarez, D. R., Roman-Cuesta, R. M., Saatchi, S. S., Slay, C. M., Turubanova, S. A., and Tyukavina, A.: Global maps of twenty-first century forest carbon fluxes, Nat. Clim. Change, 11, 234–240, https://doi.org/10.1038/s41558-020-00976-6, 2021.

Hermann, M., Röthlisberger, M., Gessler, A., Rigling, A., Senf, C., Wohlgemuth, T., and Wernli, H.: Meteorological history of low-forest-greenness events in Europe in 2002–2022, Biogeosciences, 20, 1155–1180, https://doi.org/10.5194/bg-20-1155-2023, 2023.

Hikino, K., Danzberger, J., Riedel, V. P., Rehschuh, R., Ruehr, N. K., Hesse, B. D., Lehmann, M. M., Buegger, F., Weikl, F., Pritsch, K., and Grams, T. E. E.: High resilience of carbon transport in long-term drought-stressed mature Norway spruce trees within 2 weeks after drought release, Glob. Change Biol., 28, 2095–2110, https://doi.org/10.1111/gcb.16051, 2022a.

Hikino, K., Danzberger, J., Riedel, V. P., Hesse, B. D., Hafner, B. D., Gebhardt, T., Rehschuh, R., Ruehr, N. K., Brunn, M., Bauerle, T. L., Landhäusser, S. M., Lehmann, M. M., Rötzer, T., Pretzsch, H., Buegger, F., Weikl, F., Pritsch, K., and Grams, T. E. E.: Dynamics of initial carbon allocation after drought release in mature Norway spruce-Increased belowground allocation of current photoassimilates covers only half of the carbon used for fine-root growth, Glob. Change Biol., 28, 6889–6905, https://doi.org/10.1111/gcb.16388, 2022b.

Hildebrandt, A.: Root-water relations and interactions in mixed forest settings, Forest-Water Interactions, 240, 319–348, https://doi.org/10.1007/978-3-030-26086-6_14, 2020.

Högberg, P., Nordgren, A., Buchmann, N., Taylor, A. F. S., Ekblad, A., Högberg, M. N., Nyberg, G., Ottosson-Löfvenius, M., and Read, D. J.: Large-scale forest girdling shows that current photosynthesis drives soil respiration, Nature, 411, 789–792, https://doi.org/10.1038/35081058, 2001.

Högberg, P., Högberg, M. N., Göttlicher, S. G., Betson, N. R., Keel, S. G., Metcalfe, D. B., Campbell, C., Schindlbacher, A., Hurry, V., Lundmark, T., Linder, S., and Näsholm, T.: High temporal resolution tracing of photosynthate carbon from the tree canopy to forest soil microorganisms, New Phytol., 177, 220–228, https://doi.org/10.1111/j.1469-8137.2007.02238.x, 2008.

Horst, T. W.: A simple formula for attenuation of eddy fluxes measured with first-order-response scalar sensors, Bound.-Lay. Meteorol., 82, 219–233, https://doi.org/10.1023/A:1000229130034, 1997.

Hothorn, T., Hornik, K., and Zeileis, A.: Unbiased recursive partitioning: A conditional inference framework, J. Comput. Graph. Stat., 15, 651–674, https://doi.org/10.1198/106186006x133933, 2006.

Ionita, M., Tallaksen, L. M., Kingston, D. G., Stagge, J. H., Laaha, G., Van Lanen, H. A. J., Scholz, P., Chelcea, S. M., and Haslinger, K.: The European 2015 drought from a climatological perspective, Hydrol. Earth Syst. Sci., 21, 1397–1419, https://doi.org/10.5194/hess-21-1397-2017, 2017.

Ionita, M., Dima, M., Nagavciuc, V., Scholz, P., and Lohmann, G.: Past megadroughts in central Europe were longer, more severe and less warm than modern droughts, Communications Earth & Environment, 2, 61, https://doi.org/10.1038/s43247-021-00130-w, 2021.

IPCC: Climate Change 2022 – Impacts, Adaptation and Vulnerability. Contribution of Working Group II to the Sixth Assessment Report of the Intergovernmental Panel on Climate Change, Cambridge University Press, Cambridge, UK and New York, NY, USA, 3056, https://doi.org/10.1017/9781009325844, 2023.

Janssens, I. A., Lankreijer, H., Matteucci, G., Kowalski, A. S., Buchmann, N., Epron, D., Pilegaard, K., Kutsch, W., Longdoz, B., Grünwald, T., Montagnani, L., Dore, S., Rebmann, C., Moors, E. J., Grelle, A., Rannik, Ü., Morgenstern, K., Oltchev, S., Clement, R., Gudmundsson, J., Minerbi, S., Berbigier, P., Ibrom, A., Moncrieff, J., Aubinet, M., Bernhofer, C., Jensen, N. O., Vesala, T., Granier, A., Schulze, E. D., Lindroth, A., Dolman, A. J., Jarvis, P. G., Ceulemans, R., and Valentini, R.: Productivity overshadows temperature in determining soil and ecosystem respiration across European forests, Glob. Change Biol., 7, 269–278, https://doi.org/10.1046/j.1365-2486.2001.00412.x, 2001.

Jassal, R. S., Black, T. A., Novak, M. D., Gaumont-Guay, D., and Nesic, Z.: Effect of soil water stress on soil respiration and its temperature sensitivity in an 18-year-old temperate Douglas-fir stand, Glob. Change Biol., 14, 1305–1318, https://doi.org/10.1111/j.1365-2486.2008.01573.x, 2008.

Jiao, T., Williams, C. A., De Kauwe, M. G., Schwalm, C. R., and Medlyn, B. E.: Patterns of post-drought recovery are strongly influenced by drought duration, frequency, post-drought wetness, and bioclimatic setting, Glob. Change Biol., 27, 4630–4643, https://doi.org/10.1111/gcb.15788, 2021.

Kim, J. B., So, J. M., and Bae, D. H.: Global Warming impacts on severe drought characteristics in Asia monsoon region, Water, 12, 1360, https://doi.org/10.3390/w12051360, 2020.

Kittler, F., Eugster, W., Foken, T., Heimann, M., Kolle, O., and Göckede, M.: High-quality eddy-covariance CO_2 budgets under cold climate conditions, J. Geophys. Res.-Biogeo., 122, 2064–2084, https://doi.org/10.1002/2017jg003830, 2017.

Knohl, A., Soe, A. R. B., Kutsch, W. L., Göckede, M., and Buchmann, N.: Representative estimates of soil and ecosystem respiration in an old beech forest, Plant Soil, 302, 189–202, https://doi.org/10.1007/s11104-007-9467-2, 2008.

Körner, C., Möhl, P., and Hiltbrunner, E.: Four ways to define the growing season, Ecol. Lett., 26, 1277–1292, https://doi.org/10.1111/ele.14260, 2023.

Kumarathunge, D. P., Medlyn, B. E., Drake, J. E., Tjoelker, M. G., Aspinwall, M. J., Battaglia, M., Cano, F. J., Carter, K. R., Cavaleri, M. A., Cernusak, L. A., Chambers, J. Q., Crous, K. Y., De Kauwe, M. G., Dillaway, D. N., Dreyer, E., Ellsworth, D. S., Ghannoum, O., Han, Q. M., Hikosaka, K., Jensen, A. M., Kelly, J. W. G., Kruger, E. L., Mercado, L. M., Onoda, Y., Reich, P. B., Rogers, A., Slot, M., Smith, N. G., Tarvainen, L., Tissue,

D. T., Togashi, H. F., Tribuzy, E. S., Uddling, J., Vårhammar, A., Wallin, G., Warren, J. M., and Way, D. A.: Acclimation and adaptation components of the temperature dependence of plant photosynthesis at the global scale, New Phytol., 222, 768–784, https://doi.org/10.1111/nph.15668, 2019.

Lasslop, G., Reichstein, M., Papale, D., Richardson, A. D., Arneth, A., Barr, A., Stoy, P., and Wohlfahrt, G.: Separation of net ecosystem exchange into assimilation and respiration using a light response curve approach: critical issues and global evaluation, Glob. Change Biol., 16, 187–208, https://doi.org/10.1111/j.1365-2486.2009.02041.x, 2010.

Lee, M.-S., Nakane, K., Nakatsubo, T., Mo, W.-H., and Koizumi, H.: Effects of rainfall events on soil CO_2 flux in a cool temperate deciduous broad-leaved forest, Ecol. Res., 17, 401–409, https://doi.org/10.1046/j.1440-1703.2002.00498.x, 2002.

Lu, R. Y., Xu, K., Chen, R. D., Chen, W., Li, F., and Lv, C. Y.: Heat waves in summer 2022 and increasing concern regarding heat waves in general, Atmos. Oceanic Sci. Lett., 16, 100290, https://doi.org/10.1016/j.aosl.2022.100290, 2023.

Lundberg, S. M. and Lee, S. I.: A Unified Approach to interpreting model predictions, Adv. Neur. In., 30, arXiv:1705.07874, https://doi.org/10.48550/arXiv.1705.07874, 2017.

Lundberg, S. M., Erion, G., Chen, H., DeGrave, A., Prutkin, J. M., Nair, B., Katz, R., Himmelfarb, J., Bansal, N., and Lee, S. I.: From local explanations to global understanding with explainable AI for trees, Nature Machine Intelligence, 2, 56–67, https://doi.org/10.1038/s42256-019-0138-9, 2020.

Manzoni, S., Schimel, J. P., and Porporato, A.: Responses of soil microbial communities to water stress: results from a meta-analysis, Ecology, 93, 930–938, https://doi.org/10.1890/11-0026.1, 2012.

Markonis, Y., Kumar, R., Hanel, M., Rakovec, O., Máca, P., and AghaKouchak, A.: The rise of compound warm-season droughts in Europe, Science Advances, 7, eabb9668, https://doi.org/10.1126/sciadv.abb9668, 2021.

Martinez-Garcia, E., Nilsson, M. B., Laudon, H., Lundmark, T., Fransson, J. E. S., Wallerman, J., and Peichl, M.: Overstory dynamics regulate the spatial variability in forest-floor CO_2 fluxes across a managed boreal forest landscape, Agr. Forest Meteorol., 318, 108916, https://doi.org/10.1016/j.agrformet.2022.108916, 2022.

Mauder, M. and Foken, T.: Impact of post-field data processing on eddy covariance flux estimates and energy balance closure, Meteorol. Z., 15, 597–610, 2006.

MeteoSvizzera: Rapporto sul clima 2022, ISSN: 2296-1526, 2023.

Miralles, D. G., Gentine, P., Seneviratne, S. I., and Teuling, A. J.: Land-atmospheric feedbacks during droughts and heatwaves: state of the science and current challenges, Ann. N. Y. Acad. Sci., 1436, 19–35, https://doi.org/10.1111/nyas.13912, 2019.

Moncrieff, J., Clement, R., Finnigan, J., and Meyers, T.: Averaging, detrending, and filtering of eddy covariance time series, in: Handbook of Micrometeorology: A Guide for Surface Flux Measurement and Analysis, Springer, https://doi.org/10.1007/1-4020-2265-4_2, 7–31, 2004.

Netzer, F., Thöm, C., Celepirovic, N., Ivankovic, M., Alfarraj, S., Dounavi, A., Simon, J., Herschbach, C., and Rennenberg, H.: Drought effects on C, N, and P nutrition and the antioxidative system of beech seedlings depend on geographic origin, J. Plant Nutr. Soil Sc., 179, 136–150, https://doi.org/10.1002/jpln.201500461, 2016.

Nickel, U. T., Weikl, F., Kerner, R., Schäfer, C., Kallenbach, C., Munch, J. C., and Pritsch, K.: Quantitative losses vs. qualitative stability of ectomycorrhizal community responses to 3 years of experimental summer drought in a beech-spruce forest, Glob. Change Biol., 24, E560–E576, https://doi.org/10.1111/gcb.13957, 2018.

Obladen, N., Dechering, P., Skiadaresis, G., Tegel, W., Kessler, J., Höllerl, S., Kaps, S., Hertel, M., Dulamsuren, C., Seifert, T., Hirsch, M., and Seim, A.: Tree mortality of European beech and Norway spruce induced by 2018-2019 hot droughts in central Germany, Agr. Forest Meteorol., 307, 108482, https://doi.org/10.1016/j.agrformet.2021.108482, 2021.

Orth, R.: When the land surface shifts gears, AGU Advances, 2, e2021AV000414, https://doi.org/10.1029/2021AV000414, 2021.

Paul-Limoges, E., Wolf, S., Eugster, W., Hörtnagl, L., and Buchmann, N.: Below-canopy contributions to ecosystem CO_2 fluxes in a temperate mixed forest in Switzerland, Agr. Forest Meteorol., 247, 582–596, https://doi.org/10.1016/j.agrformet.2017.08.011, 2017.

Paul-Limoges, E., Wolf, S., Schneider, F. D., Longo, M., Moorcroft, P., Gharun, M., and Damm, A.: Partitioning evapotranspiration with concurrent eddy covariance measurements in a mixed forest, Agr. Forest Meteorol., 280, 107786, https://doi.org/10.1016/j.agrformet.2019.107786, 2020.

Pei, F. S., Li, X., Liu, X. P., and Lao, C. H.: Assessing the impacts of droughts on net primary productivity in China, J. Environ. Manage., 114, 362–371, https://doi.org/10.1016/j.jenvman.2012.10.031, 2013.

Petek-Petrik, A., Húdoková, H., Fleischer, P., Jamnická, G., Kurjak, D., Sliacka Konôpková, A., and Petrík, P.: The combined effect of branch position, temperature, and VPD on gas exchange and water-use efficiency of Norway spruce, Biol. Plant., 67, 136–141, https://doi.org/10.32615/bp.2023.017, 2023.

R Core Team: R: a language and environment for statistical computing, R Foundation for Statistical Computing, Vienna, 2021.

Reichstein, M., Falge, E., Baldocchi, D., Papale, D., Aubinet, M., Berbigier, P., Bernhofer, C., Buchmann, N., Gilmanov, T., Granier, A., Grünwald, T., Havránková, K., Ilvesniemi, H., Janous, D., Knohl, A., Laurila, T., Lohila, A., Loustau, D., Matteucci, G., Meyers, T., Miglietta, F., Ourcival, J. M., Pumpanen, J., Rambal, S., Rotenberg, E., Sanz, M., Tenhunen, J., Seufert, G., Vaccari, F., Vesala, T., Yakir, D., and Valentini, R.: On the separation of net ecosystem exchange into assimilation and ecosystem respiration:: review and improved algorithm, Glob. Change Biol., 11, 1424–1439, https://doi.org/10.1111/j.1365-2486.2005.001002.x, 2005.

Ruehr, N. K. and Buchmann, N.: Soil respiration fluxes in a temperate mixed forest: seasonality and temperature sensitivities differ among microbial and root-rhizosphere respiration, Tree Physiol., 30, 165–176, https://doi.org/10.1093/treephys/tpp106, 2010.

Ruehr, N. K., Offermann, C. A., Gessler, A., Winkler, J. B., Ferrio, J. P., Buchmann, N., and Barnard, R. L.: Drought effects on allocation of recent carbon: from beech leaves to soil CO_2 efflux, New Phytol., 184, 950–961, https://doi.org/10.1111/j.1469-8137.2009.03044.x, 2009.

Ruehr, N. K., Knohl, A., and Buchmann, N.: Environmental variables controlling soil respiration on diurnal, seasonal and annual time-scales in a mixed mountain forest in Switzerland, Bio-

geochemistry, 98, 153–170, https://doi.org/10.1007/s10533-009-9383-z, 2010.

Rukh, S., Sanders, T. G. M., Krüger, I., Schad, T., and Bolte, A.: Distinct responses of European beech (*Fagus sylvatica* L.) to drought intensity and length – A review of the impacts of the 2003 and 2018-2019 drought events in central Europe, Forests, 14, 248, https://doi.org/10.3390/f14020248, 2023.

Sabbatini, S., Mammarella, I., Arriga, N., Fratini, G., Graf, A., Hörtriagl, L., Ibrom, A., Longdoz, B., Mauder, M., Merbold, L., Metzger, S., Montagnani, L., Pitacco, A., Rebmann, C., Sedlák, P., Sigut, L., Vitale, D., and Papale, D.: Eddy covariance raw data processing for CO_2 and energy fluxes calculation at ICOS ecosystem stations, Int. Agrophys., 32, 495–515, https://doi.org/10.1515/intag-2017-0043, 2018.

Scapucci, L., Shekhar, A., Hörtnagl, L., and Buchmann, N.: Subcanopy eddy covariance and chamber soil respiration data, ETHZ [data set], https://doi.org/10.3929/ethz-b-000687324, 2024.

Schindlbacher, A., Wunderlich, S., Borken, W., Kitzler, B., Zechmeister-Boltenstern, S., and Jandl, R.: Soil respiration under climate change: prolonged summer drought offsets soil warming effects, Glob. Change Biol., 18, 2270–2279, https://doi.org/10.1111/j.1365-2486.2012.02696.x, 2012.

Schuldt, B. and Ruehr, N. K.: Responses of European forests to global change-type droughts, Plant Biol., 24, 1093–1097, https://doi.org/10.1111/plb.13484, 2022.

Schuldt, B., Buras, A., Arend, M., Vitasse, Y., Beierkuhnlein, C., Damm, A., Gharun, M., Grams, T. E. E., Hauck, M., Hajek, P., Hartmann, H., Hiltbrunner, E., Hoch, G., Holloway-Phillips, M., Körner, C., Larysch, E., Lübbe, T., Nelson, D. B., Rammig, A., Rigling, A., Rose, L., Ruehr, N. K., Schumann, K., Weiser, F., Werner, C., Wohlgemuth, T., Zang, C. S., and Kahmen, A.: A first assessment of the impact of the extreme 2018 summer drought on Central European forests, Basic Appl. Ecol., 45, 86–103, https://doi.org/10.1016/j.baae.2020.04.003, 2020.

Schulze E. D., Beck, E., Buchmann, N., Clemens, S., Müller-Hohenstein, K., and Scherer-Lorenzen, M. (Eds.): Plant Ecology, 2, Springer, ISBN: 978-3-662-56231-4, 928 pp. 2019.

Schwalm, C. R., Williams, C. A., Schaefer, K., Arneth, A., Bonal, D., Buchmann, N., Chen, J. Q., Law, B. E., Lindroth, A., Luyssaert, S., Reichstein, M., and Richardson, A. D.: Assimilation exceeds respiration sensitivity to drought: A FLUXNET synthesis, Glob. Change Biol., 16, 657–670, https://doi.org/10.1111/j.1365-2486.2009.01991.x, 2010.

Sendall, K. M., Reich, P. B., Zhao, C. M., Hou, J. H., Wei, X. R., Stefanski, A., Rice, K., Rich, R. L., and Montgomery, R. A.: Acclimation of photosynthetic temperature optima of temperate and boreal tree species in response to experimental forest warming, Glob. Change Biol., 21, 1342–1357, https://doi.org/10.1111/gcb.12781, 2015.

Shapley, L. S.: Stochastic Games, P. Natl. Acad. Sci. USA, 39, 1095–1100, https://doi.org/10.1073/pnas.39.10.1095, 1953.

Shekhar, A., Chen, J., Bhattacharjee, S., Buras, A., Castro, A. O., Zang, C. S., and Rammig, A.: Capturing the impact of the 2018 European drought and heat across different vegetation types using OCO-2 Solar-Induced Fluorescence, Remote Sens.-Basel, 12, 3249, https://doi.org/10.3390/rs12193249, 2020.

Shekhar, A., Hörtnagl, L., Gharun, M., and Buchmann, N.: CH-LAE FP2022 (2004–2022): Ecosystem fluxes and meteorological data from Lägeren, Switzerland, ETHZ [data set], https://doi.org/10.3929/ethz-b-000582198, 2022.

Shekhar, A., Buchmann, N., Humphrey, V., and Gharun, M.: More than three-fold increase in compound soil and air dryness across Europe by the end of 21st century, Weather Clim. Extrem., 44, 100666, https://doi.org/10.21203/rs.3.rs-3143908/v2, 2024.

Shekhar, A., Hörtnagl, L., Paul-Limoges, E., Etzold, S., Zweifel, R., Buchmann, N., and Gharun, M.: Contrasting impact of extreme soil and atmospheric dryness on the functioning of trees and forests, Sci. Total Environ., 916, 169931, https://doi.org/10.1016/j.scitotenv.2024.169931, 2024.

Smith, N. G. and Dukes, J. S.: Short-term acclimation to warmer temperatures accelerates leaf carbon exchange processes across plant types, Glob. Change Biol., 23, 4840–4853, https://doi.org/10.1111/gcb.13735, 2017.

Sperlich, D., Chang, C. T., Peñuelas, J., and Sabaté, S.: Responses of photosynthesis and component processes to drought and temperature stress: are Mediterranean trees fit for climate change?, Tree Physiol., 39, 1783–1805, https://doi.org/10.1093/treephys/tpz089, 2019.

Spinoni, J., Vogt, J. V., Naumann, G., Barbosa, P., and Dosio, A.: Will drought events become more frequent and severe in Europe?, Int. J. Climatol., 38, 1718–1736, https://doi.org/10.1002/joc.5291, 2018.

Strobl, C., Boulesteix, A.-L., Kneib, T., Augustin, T., and Zeileis, A.: Conditional variable importance for random forests, BMC Bioinform., 9, 1–11, 2008.

Sun, S. Q., Lei, H. Q., and Chang, S. X.: Drought differentially affects autotrophic and heterotrophic soil respiration rates and their temperature sensitivity, Biol. Fert. Soils, 55, 275–283, https://doi.org/10.1007/s00374-019-01347-w, 2019.

Talmon, Y., Sternberg, M., and Grünzweig, J. M.: Impact of rainfall manipulations and biotic controls on soil respiration in Mediterranean and desert ecosystems along an aridity gradient, Glob. Change Biol., 17, 1108–1118, https://doi.org/10.1111/j.1365-2486.2010.02285.x, 2011.

Tripathy, K. P. and Mishra, A. K.: How Unusual Is the 2022 European Compound Drought and Heatwave Event?, Geophys. Res. Lett., 50, e2023GL105453, https://doi.org/10.1029/2023GL105453, 2023.

van der Molen, M. K., Dolman, A. J., Ciais, P., Eglin, T., Gobron, N., Law, B. E., Meir, P., Peters, W., Phillips, O. L., Reichstein, M., Chen, T., Dekker, S. C., Doubkova, M., Friedl, M. A., Jung, M., van den Hurk, B. J. J. M., de Jeu, R. A. M., Kruijt, B., Ohta, T., Rebel, K. T., Plummer, S., Seneviratne, S. I., Sitch, S., Teuling, A. J., van der Werf, G. R., and Wang, G.: Drought and ecosystem carbon cycling, Agr. Forest Meteorol., 151, 765–773, https://doi.org/10.1016/j.agrformet.2011.01.018, 2011.

van der Woude, A. M., Peters, W., Joetzjer, E., Lafont, S., Koren, G., Ciais, P., Ramonet, M., Xu, Y. D., Bastos, A., Botia, S., Sitch, S., de Kok, R., Kneuer, T., Kubistin, D., Jacotot, A., Loubet, B., Herig-Coimbra, P. H., Loustau, D., and Luijkx, I. T.: Temperature extremes of 2022 reduced carbon uptake by forests in Europe, Nat. Commun., 14, 6218, https://doi.org/10.1038/s41467-023-41851-0, 2023.

van Straaten, O., Veldkamp, E., and Corre, M. D.: Simulated drought reduces soil CO_2 efflux and production in a tropical forest in Sulawesi, Indonesia, Ecosphere, 2, 1–22, https://doi.org/10.1890/Es11-00079.1, 2011.

von Buttlar, J., Zscheischler, J., Rammig, A., Sippel, S., Reichstein, M., Knohl, A., Jung, M., Menzer, O., Arain, M. A., Buchmann, N., Cescatti, A., Gianelle, D., Kiely, G., Law, B. E., Magliulo, V., Margolis, H., McCaughey, H., Merbold, L., Migliavacca, M., Montagnani, L., Oechel, W., Pavelka, M., Peichl, M., Rambal, S., Raschi, A., Scott, R. L., Vaccari, F. P., van Gorsel, E., Varlagin, A., Wohlfahrt, G., and Mahecha, M. D.: Impacts of droughts and extreme-temperature events on gross primary production and ecosystem respiration: a systematic assessment across ecosystems and climate zones, Biogeosciences, 15, 1293–1318, https://doi.org/10.5194/bg-15-1293-2018, 2018.

Wang, H., Yan, S. J., Ciais, P., Wigneron, J. P., Liu, L. B., Li, Y., Fu, Z., Ma, H. L., Liang, Z., Wei, F. L., Wang, Y. Y., and Li, S. C.: Exploring complex water stress-gross primary production relationships: Impact of climatic drivers, main effects, and interactive effects, Glob. Change Biol., 28, 4110–4123, https://doi.org/10.1111/gcb.16201, 2022.

Wang, Y. F., Hao, Y. B., Cui, X. Y., Zhao, H. T., Xu, C. Y., Zhou, X. Q., and Xu, Z. H.: Responses of soil respiration and its components to drought stress, J. Soil. Sediment., 14, 99–109, https://doi.org/10.1007/s11368-013-0799-7, 2014.

Webb, E. K., Pearman, G. I., and Leuning, R.: Correction of Flux Measurements for Density Effects Due to Heat and Water-Vapor Transfer, Q. J. Roy. Meteor. Soc., 106, 85–100, https://doi.org/10.1002/qj.49710644707, 1980.

Xu, B., Arain, M. A., Black, T. A., Law, B. E., Pastorello, G. Z., and Chu, H. S.: Seasonal variability of forest sensitivity to heat and drought stresses: A synthesis based on carbon fluxes from North American forest ecosystems, Glob. Change Biol., 26, 901–918, https://doi.org/10.1111/gcb.14843, 2020.

Yao, Y., Liu, Y. X., Zhou, S., Song, J. X., and Fu, B. J.: Soil moisture determines the recovery time of ecosystems from drought, Glob. Change Biol., 29, 3562–3574, https://doi.org/10.1111/gcb.16620, 2023.

Zheng, P. F., Wang, D. D., Yu, X. X., Jia, G. D., Liu, Z. Q., Wang, Y. S., and Zhang, Y. G.: Effects of drought and rainfall events on soil autotrophic respiration and heterotrophic respiration, Agr. Ecosyst. Environ., 308, 107267, https://doi.org/10.1016/j.agee.2020.107267, 2021.

Zhou, S., Williams, A. P., Berg, A. M., Cook, B. I., Zhang, Y., Hagemann, S., Lorenz, R., Seneviratne, S. I., and Gentine, P.: Land-atmosphere feedbacks exacerbate concurrent soil drought and atmospheric aridity, P. Natl. Acad. Sci. USA, 116, 18848–18853, https://doi.org/10.1073/pnas.1904955116, 2019.

Zomer, R. J., Xu, J., and Trabucco, A.: Version 3 of the global aridity index and potential evapotranspiration database, Sci. Data, 9, 409, https://doi.org/10.1038/s41597-022-01493-1, 2022.